

Accepted Manuscript

Geological setting and paleomagnetism of the Eocene red beds of Laguna Brava Formation (Quebrada Santo Domingo, northwestern Argentina)

H. Vizán, S. Geuna, R. Melchor, E.S. Bellosi, S.L. Lagorio, C. Vásquez, M.S. Japas, G. Ré, M. Do Campo

PII: S0040-1951(12)00690-7
DOI: doi: [10.1016/j.tecto.2012.10.026](https://doi.org/10.1016/j.tecto.2012.10.026)
Reference: TECTO 125662

To appear in: *Tectonophysics*

Received date: 8 August 2012
Revised date: 4 October 2012
Accepted date: 24 October 2012



Please cite this article as: Vizán, H., Geuna, S., Melchor, R., Bellosi, E.S., Lagorio, S.L., Vásquez, C., Japas, M.S., Ré, G., Do Campo, M., Geological setting and paleomagnetism of the Eocene red beds of Laguna Brava Formation (Quebrada Santo Domingo, northwestern Argentina), *Tectonophysics* (2012), doi: [10.1016/j.tecto.2012.10.026](https://doi.org/10.1016/j.tecto.2012.10.026)

This is a PDF file of an unedited manuscript that has been accepted for publication. As a service to our customers we are providing this early version of the manuscript. The manuscript will undergo copyediting, typesetting, and review of the resulting proof before it is published in its final form. Please note that during the production process errors may be discovered which could affect the content, and all legal disclaimers that apply to the journal pertain.

**Geological setting and paleomagnetism of the Eocene red beds of
Laguna Brava Formation (Quebrada Santo Domingo, northwestern
Argentina)**

Vizán, H.^{1*}, Geuna, S.¹, Melchor, R.², Bellosi, E.S.³, Lagorio, S.L.⁴, Vásquez,
C.^{1,5}, Japas, M.S.¹, Ré, G.¹, Do Campo, M.⁶

¹ IGEBA (CONICET – UBA), Departamento de Ciencias Geológicas, Facultad de Ciencias Exactas y Naturales, Universidad de Buenos Aires. Ciudad Universitaria, Pabellón 2, 1428 Ciudad Autónoma de Buenos Aires, Argentina.

² INCITAP (CONICET and Universidad Nacional de La Pampa), Av. Uruguay 151, 6300 Santa Rosa, La Pampa, Argentina.

³ CONICET- División Icnología, Museo Argentino de Ciencias Naturales, Av. Ángel Gallardo 470, 1405 Ciudad Autónoma de Buenos Aires, Argentina.

⁴ Servicio Geológico Minero Argentino, J.A. Roca 651 Piso 10°. 1067 Ciudad Autónoma de Buenos Aires, Argentina.

⁵ Ciclo Básico Común, Universidad de Buenos Aires, Ciudad Universitaria, 1428 Ciudad Autónoma de Buenos Aires.

⁶ INGEIS (CONICET – UBA), Ciudad Universitaria, 1428 Ciudad Autónoma de Buenos Aires, Argentina.

- Corresponding author: e-mail haroldo@gl.fcen.uba.ar, Tel/Fax. 54-1145763300 ext 292,

Abstract

The red bed succession cropping out in the Quebrada Santo Domingo in northwestern Argentina had been for long considered as Upper Triassic-Lower Jurassic in age based in weak radiometric and paleontological evidence. Preliminary paleomagnetic data confirmed the age and opened questions about the nature of fossil footprints with avian features discovered in the section. Recently the stratigraphic scheme was reviewed with the identification of previously unrecognized discontinuities, and a radiometric dating obtained in a tuff, indicated an Eocene age for the Laguna Brava Formation and the fossil bird footprints, much younger than the previously assigned. We present a detailed paleomagnetic study interpreted within a regional tectonic and stratigraphic framework, looking for an explanation for the misinterpretation of the preliminary paleomagnetic data.

The characteristic remanent magnetizations pass a tilt test and a reversal test. The main magnetic carrier is interpreted to be low Ti titanomagnetite and to a lesser extent hematite. The characteristic remanent magnetization would be essentially detrital. The obtained paleomagnetic pole (PP) for the Laguna Brava Formation has the following geographic coordinates and statistical parameters: $N=29$, $Lon.=184.5^\circ E$, $Lat.=75.0^\circ S$, $A95=5.6^\circ$, $K=23.7$. When this PP is compared with another one with similar age obtained in an undeformed area, a declination anomaly is recognized. This anomaly can be interpreted as Laguna Brava Formation belonging to a structural block that rotated about 16° clockwise along a vertical axis after about 34 Ma. This block rotation is consistent with the regional tectonic framework, and would have caused the fortuitous coincidence of the PP with Early Jurassic poles. According to the interpreted magnetostratigraphic correlation, the Laguna Brava Formation would have been

deposited during the Late Eocene with a mean sedimentation rate of about 1.4 cm per thousand years, probably in relation to the onset of the Andean deformation.

Keywords: Paleomagnetism; red beds; Triassic-Jurassic; Eocene; block rotations; magnetostratigraphy

1. Introduction

The discovery of fossil footprints with avian features by Melchor et al. (2002) generated several questions regarding the age of the host rocks and of their likely producer, with significant implications for the origin and evolution of birds. The small, bird-like footprints were collected from a section at Quebrada Santo Domingo (La Rioja Province, Argentina) that is composed by a thick red bed succession with interbedded basalt flows. The age of the footprint-bearing section was first considered Late Triassic because the lower part of the section has yielded remains of *Rhexoxylon* (Caminos et al., 1995), a wood morphogenus only reported from Middle to Upper Triassic rocks of Gondwana (Artabe et al., 1999), and the basalt flows, located below the bed with the bird-like footprints, yielded an $^{40}\text{Ar}/^{39}\text{Ar}$ age of 212.5 ± 7.0 Ma (Coughlin, 2000).

A new detailed geological study indicated that the basalt flows were stratigraphically repeated by tectonic structures and located the outcrop of these volcanic rocks and the unit with *Rhexoxylon* below the beds with bird-like footprints (i.e. Vizán et al., 2005). A preliminary paleomagnetic study was then carried out to constrain the age of the deposits and the obtained paleopole was in agreement with Early Jurassic tracks of different apparent polar wander paths (Vizán et al., 2005).

The presence of flight trace fossils associated with probing marks and a similar morphology of the fossil bird-like footprints with tracks of modern shorebirds, strongly suggest an avian affinity for the producers of the tracks (Genise et al., 2009). The close correspondence of ancient footprints with those of present-day sandpipers created a conundrum: the most primitive birds have similar behaviors to the modern ones? This evidence casts doubts about the Late Triassic-Early Jurassic age of the hosting Quebrada Santo Domingo succession, which would be probably younger if it has to match the known body fossil record of birds.

Considering that paleomagnetic data can suggest but not determine chronological ages, radiometric dating was applied in a tuff interbedded in the stratigraphic section that includes the unit with the fossil tracks, resulting in an age of about 37 Ma (Melchor et al., submitted). The obtained age is substantially younger than the Mesozoic age previously thought, and it opens a new question about the meaning of the geographic position of the preliminary paleopole.

A complete paleomagnetic study of different sections of red beds outcropping at Quebrada Santo Domingo (Figs. 1 and 2) is conducted in this paper. The results are reviewed in the light of the new radiometric and geological evidence, and reinterpreted within a regional tectonic and stratigraphic framework. It is concluded that the coincidence of the paleomagnetic pole with Early Jurassic paths, previously considered as a further evidence of the Early Mesozoic age of the strata, might have been fortuitous and caused by a tectonic rotation of the area in recent times. This turns to be an excellent example of the importance of establishing the structural control and tectonic coherence with neighboring blocks in paleomagnetic studies, as local rotations can be commonplace and easily overlooked in orogenic belts.

2. Geological setting

The red bed succession of the Quebrada Santo Domingo area (Figs. 1, 2, 3) has been previously referred to the Santo Domingo Formation (Coughlin, 2000; Caminos and Fauqué, 2001). Garrone et al. (2008) distinguished two units separated by an angular unconformity in the former Santo Domingo Formation: a lower coarser-grained succession that was assigned to the Quebrada Santo Domingo Formation (Late Triassic-Early Jurassic) and an overlying succession assigned to the Laguna Brava Formation. The age of the Laguna Brava Formation was considered Cretaceous by Garrone et al.

(2008) on the basis of poorly preserved bone remains found by Coughlin (2000) that were identified as titanosaurid sauropod remains by Arcucci et al. (2005). The age of the Laguna Brava Formation is now considered Late Eocene on the basis of a new date from zircon grains of a tuff layer of the unit (Melchor et al., submitted), while the significance of the sauropod remains has yet to be explained. The red bed succession of the Quebrada de Santo Domingo area is bounded by reverse faults. The package contains at least two internal thrust faults and several folds, including overturned synclines near the thrust faults (Fig. 2). Major faults and folds are roughly southwest-northeast oriented. The sections measured for this work (A to F in Fig. 2) are located in a single thrust sheet.

To better understand the stratigraphy of the units outcropping in Quebrada Santo Domingo area that are analyzed in this paper, a detailed description is presented below.

2.1. Quebrada Santo Domingo Formation

The basal boundary is faulted and lies on Carboniferous volcanic rocks. The Quebrada Santo Domingo Formation is 1100 m thick (sections A and B in Figs. 2 and 3) and is divided into five facies associations (FA), representing alluvial fans, ephemeral braided rivers and shallow lakes developed in semiarid to arid conditions. The lower FA (260 m, FA1, Fig. 3) comprises large lobate bodies (10-25 m thick and 50-300 m long) of massive, stratified or cross-bedded conglomerates (maximum clast size 0.50 m) with imbricated clasts, along with cross-bedded or massive gravelly sandstones, embedded in laminated and cross-bedded, medium-fine sandstones and mudstones. The last facies includes scarce, very-weakly developed paleosols with mottles and root traces. Large silicified remains of transported logs corresponding to *Rhexoxylon* and *Taxaceoxylon* (Caminos et al., 1995) occur in coarse lobes. This fining-

upward FA records sedimentation in proximal to distal alluvial fans. The following FA (345 m, FA2, Fig. 3) was deposited in a braided river setting which flowed to the SW. It includes lenticular bodies composed of fining-upward cycles (5-20 m) conglomerates and coarse to fine, pink sandstones showing through-cross bedding or parallel lamination accumulated in channels. Thick beds of laminated mudstones and sandstones, along with few weakly-developed non-calcareous paleosols, represent extended floodplain deposits and lacustrine facies probably accumulated in a rapid-subsiding basin. The third FA (90 m, FA3, Fig. 3) is a well-stratified coarsening-upward succession, dark red in color, accumulated in a shallow lacustrine system. It is composed of tabular beds of ripple-laminated fine-grained sandstone that pass upward to cross-bedded and laminated medium-grained sandstone, showing frequent desiccation cracks and bioturbation. Asymmetrical ripples indicate SE paleocurrents. The fourth FA (310 m, FA4, Fig. 3) comprises fluvial deposits including cross-bedded (paleocurrents to the SE) and laminated fine to medium-grained sandstones in the lower part (100 m), overlain by cross-bedded or massive, coarse and gravelly sandstones and fine conglomerates. This FA includes four dark grey flows of alkaline basalts (see sections 3.2. and 4.3.1.) with abundant vesicles, which are up to 16 m thick. The top of each lava flow is weathered, while the top of the uppermost basalt is eroded and intensely calcretized. These basalt lava flows were dated as Late Triassic (Coughlin, 2000). Common, massive, nodular, laminated or prismatic pedogenic calcrete with root traces and burrows occurs in FA4. Proportion and thickness of calcrete horizons increase towards the top of the section. Finally, the uppermost FA of the formation (95 m, FA5, Fig. 3) is a well-stratified red colored succession deposited in fluvial channels and floodplains. It is composed of medium to coarse-grained sandstones with trough cross-bedding, laminated fine-grained sandstones, thin and scarce calcrete horizons and

subordinated mudstones. Weakly-developed paleosols, showing thin argillic subsurface horizons, rhizoconcretions, mottles and carbonate nodules were observed. In the upper part, it is recognized a distinct light grey interval (25 m) of coarse quartz sandstones with trough cross-bedding indicating NE paleocurrents.

2.2. Laguna Brava Formation

The transition from the underlying unit is subtle, marked by a facies change and locally by a gentle unconformity as pointed by Garrone et al. (2008). The change in sedimentary facies is revealed by the transition from a sandstone-dominated interval with calcrete (underlying unit) to a mudstone-dominated section. Two broad mappable intervals can be distinguished in the Laguna Brava Formation (Fig. 2): a lower fluvio-lacustrine interval (560 m thick) and an upper eolian interval (minimum thickness of 130 m). The fluvio lacustrine interval can be further divided into a 280 m thick lower lacustrine facies association (FA6, Fig. 3), an intermediate 100 m thick fluvial channel section (FA7, Fig. 3) and a 185 m thick upper lacustrine and ephemeral fluvial section (FA8, Figs. 3 and 4). The sedimentology and trace fossils of the upper lacustrine and ephemeral fluvial interval was treated in detail by Melchor et al. (2006). Described trace fossils include the bird tracks *Gruipeda dominguensis*, cf. *Alaripeda* isp. and an identified bird-like track type C (Melchor et al., 2002; De Valais and Melchor, 2008; Genise et al., 2009). The 0.12 m thick dated tuff is located at 1525 m from the base of the red bed succession (Fig. 4). Petrographic examination of a thin section of the crystal tuff suggests absence of detrital minerals, and dominance of fresh subhedral plagioclase crystals and oversized biotite crystals (Supplement Fig. S1a, b). The analysis of 7 single zircon grains yielded a weighted-mean $^{206}\text{Pb}/^{238}\text{U}$ date of $37.313 \pm 0.017/0.040/0.057$ Ma (internal uncertainties/with tracer calibration uncertainties/with decay constant

uncertainties; MSWD = 1.2) (Melchor et al., submitted). As the analyzed zircon grains (which are abundant in the sample) are exactly the same age, the possibility of a detrital contamination is unlikely. In consequence, the maximum age for the bird tracks of the Laguna Brava Formation of northwest Argentina (including *G. dominguensis*) is Late Eocene (Bartonian/Priabonian after Gradstein et al., 2004). The measured stratigraphic section of the Laguna Brava Formation is in the same thrust sheet as the bird tracks and dated tuff layer (sections B to F in Fig. 2). In addition, although the contact between the fluvio-lacustrine (FA6 to FA8) and eolian interval of the unit (FA9) is commonly by faulting, there is a section in the Quebrada Santo Domingo area (“F” in Fig. 2) where the passage between both intervals is transitional. The eolian section (FA9, Fig. 3) is dominated by fine-grained and well-sorted sandstones arranged in high-angle, asymptotic, cross-stratified beds. Set thickness range from 1.2 to 3.5 m. Low-angle and very continuous truncation surfaces were observed in the section. Garrone et al. (2008) indicate a maximum thickness of 530 m for the eolian section.

The presence of purported titanosaur remains in the fluvio-lacustrine interval of the Laguna Brava Formation is puzzling, although the remains were found in a different thrust sheet than the bird tracks and dated tuff (Fig. 2). The package with the sauropod remains is mudstone-dominated, partly covered, sheared and bounded by reverse faults. This package is provisionally mapped as part of the Laguna Brava Formation (Fig. 2). However, if the assignment of the bone remains to titanosaur sauropod is confirmed, the more parsimonious explanation is to consider that package as part of a Cretaceous unit.

3. Petrographic and geochemical data

In order to characterize the rocks sampled for paleomagnetic studies (Figs. 3, 4), petrographic, X ray diffractometry studies were carried out on the sedimentary rocks of the Laguna Brava Formation. The petrography and geochemistry (trace element) of basalts of the Quebrada Santo Domingo Formation were also studied.

3.1. Petrography and XRD of sandstones from Laguna Brava Formation

Packing parameters reflect the alterations of sandstone fabric that results from mechanical compaction, essentially characterized by the reorientation and repacking of brittle grains and by plastic deformation of ductile grains. For this study, two packing parameters were quantified: (1) the contact index (CI) or the average number of grain contacts (Taylor, 1950); (2) the tight packing index (TPI) which is the average per grain abundance of long, embayed, and sutured contacts (Wilson and McBride, 1988). These parameters were estimated by counting the types of contacts of 100 grains per thin section. In addition, the sorting of analyzed samples was estimated using the visual comparators of Harrel (1984) and the sandstone composition was approximated by counting all the grains in five random microscope fields for each sample, which resulted in 120 to 200 grains counted by thin section.

The sedimentary rocks of the Laguna Brava Formation sampled for paleomagnetic studies are essentially very-fine and fine-grained sandstones. Most samples are well-sorted, whereas moderately-sorted and very well-sorted samples are also present (Supplement Table S1). Using Folk et al.'s (1970) classification, most samples are lithic arkoses (n= 6) and the remaining are feldspathic litharenites (n= 5, Supplement Table S1). Most of the samples come from FA8 (lacustrine and ephemeral fluvial deposits), whereas a single sample was analyzed from FA9 (# 228, eolian section). The average composition of the sandstones from FA8 is Q₇:F₅₀:L₄₃. Lithic

grains are dominated by intermediate to basic volcanic fragments, whereas feldspar is essentially plagioclase. The single sample from the eolian section exhibits a contrasting composition ($Q_{30}:F_{30}:L_{40}$), with greater participation of quartz (including polycrystalline quartz) and a significant proportion of low-grade metamorphic lithic grains in addition to volcanic grains. For all analyzed samples the contact index ranges from 2.84 to 3.73 (mean 3.19, $n=11$) and the tight packing index from 0.31 to 1.10 (mean 0.68, $n=11$) (Supplement Table S1). The range of packing observed in the analyzed sandstones is exemplified by sample D1, showing an open packing and significant pore space, and sample D57 with a closer packing and reduced pore space. Red hematite is the main cement, in some cases appearing as an isopachous cement, whereas zeolite and calcite were observed in minor proportion (see Supplement Fig. S1).

Holocene fluvial sandstones have a CI that range from 0.40 to 1.80 (Atkins and McBride, 1992), which are considerably lower than the analyzed samples. Comparison of the packing indexes with similar parameters from fluvio-deltaic deposits of the Eocene Wilcox Sandstone buried at different depths (Fig. 4 in McBride et al., 1991) suggests a range of probable burial depths for the analyzed interval of the Laguna Brava Formation. Using the CI values, the estimated burial depth is 1200-2300 m, whereas a 900-1600 m range can be inferred from the TPI values (in both cases using the logarithmic regression of McBride et al., 1991). The Wilcox sandstones display an average composition of $Q_{52}:F_{16}:L_{32}$ (McBride et al., 1991). The Laguna Brava sandstones have a much lower participation of quartz and greater amount of lithic grains. These differences suggest that ductile deformation of lithic grains (e.g., Pittman and Larese, 1991) is more important in the Laguna Brava Formation than in the Wilcox sandstones. It is likely that most compaction in the Laguna Brava Formation sandstones was accommodated by ductile grain deformation, instead of grain re-orientation

(McBride et al., 1991). In consequence, the estimates of burial depth for the Laguna Brava Formation are considered as maximum values.

Petrographic analysis using reflected light shows that relic (titano)magnetite can be distinguished in many clasts, as part of an original trellis-texture, where (titano)hematite is found as alteration (martite). Other clasts with stronger oxidation show the original (titano)magnetite completely replaced by (titano)hematite (Supplement Fig. S2).

X-ray diffraction (XRD) analysis of bulk samples and clay mineral analysis of the $< 2 \mu\text{m}$ sub-fraction were performed for selected samples from the Laguna Brava Formation to distinguish the main mineral phases. Clay sub-samples ($< 2\mu\text{m}$; 13 samples) were prepared in accordance with the guidelines of Moore and Reynolds (1989). Clay minerals were identified according to the position of the (001) series of basal reflections on XRD patterns of air-dried, ethylene-glycolated, and heated specimens (at 500°C for 4 hours).

In addition to quartz and plagioclase XRD indicates the occurrence of zeolites in all the analyzed whole rocks and clay sub-samples, whereas minor calcite is present in some of them. Zeolites comprise heulandite and/or analcime, plus mordenite in a single sample (Supplement Table S2). Clinoptilolite and heulandite could not be unequivocally identified by XRD, but the collapse by heating, indicates that heulandite is the zeolite of our samples (see Bish and Boak, 2001). Common clay minerals recognized in the samples are smectite and illite (Supplement Table S2). The mineral assemblage smectite + heulandite + analcime is common in saline-alkaline lake setting, as suggested by the hosting sedimentary facies which were interpreted as an evaporitic mudflat (facies association C1 of Melchor et al., 2006). There is general agreement that in saline-alkaline lakes analcime forms by replacement of earlier zeolites, including heulandite,

with the increase of salinity and alkalinity (Wilkin and Barnes, 1998, Chipera and Apps, 2001). Although mordenite is less common than clinoptilolite-heulandite in saline-alkaline lakes, research on the kinetics and mechanisms of analcime formation from Na-clinoptilolite and Na-mordenite indicates that the latter mineral is similar to Na-clinoptilolite in both composition and solubility (Wilkin and Barnes, 2000). Volcanic glass is the most common precursor of zeolites in saline-alkaline lakes (Surdam and Sheppard, 1978; Boles and Surdam, 1979), but these minerals can also form at the expense of clay minerals, feldspars, and feldspathoids (Hay and Sheppard, 2001). Zeolites display a marked depth zonation which is strongly controlled by geothermal gradient and pore-water chemistry (Iijima and Utada, 1966; Iijima, 1988). The association of heulandite and analcime with presence of smectite is related to top of zone IIIa of Iijima (1988), which corresponds to about 84-91°C in marine basins. For continental basins the transformations can occur at lower temperatures (Iijima, 1988). Assuming a normal subduction for the area previous to 16 Ma (Ramos et al., 2002), a geothermal gradient of 30°C/km, and a mean surface temperature of 20°C, the minimum burial depth for the analyzed samples of the Laguna Brava Formation would be 2400 m. These inferences are in agreement with similar estimates from sandstone packing.

3.2. Petrography and geochemistry of Upper Triassic basalts

The four basaltic flows interbedded in the Quebrada Santo Domingo Formation (Fig. 3) display porphyritic texture composed of olivine phenocrysts (strongly altered to iddingsite) set in an intergranular groundmass of labradoritic plagioclase (An₆₃), clinopyroxene, olivine and strongly martitized titanomagnetite. Calcite-bearing amygdales are very frequent. This feature, as well as the oxidation of the mafic phases,

are both related to the late subaerial deuteric process that strongly affected the rocks. Chemical analyses were carried out in four rocks of the different sampled flows-sites (D36, D37, D38 and D39, Fig. 3). All of them show very high (> 6%) loss on ignition (LOI), as a consequence of the alteration above mentioned. Therefore only immobile trace elements have been considered.

The analyzed samples can be classified as alkali basalts in Nb/Y versus Zr/TiO₂ diagram (Winchester and Floyd, 1977), from intraplate settings (Zr-Nb-Y plot; Meschede, 1986) (Fig. 5a, b). Sample D38 is characterized by higher Zr, Nb, Y, Ti, Ta, Hf and REE contents than the other analyzed rocks (Fig. 5c). These geochemical differences suggest that one of the lava flows (site D38) is clearly different from the others, also diverging in its paleomagnetic signature (as seen in section 4.3.1).

4. Paleomagnetic sampling and experimental procedure

4.1. General methodologies

Three to four hand or block paleomagnetic samples were taken in every site. Orientation was accomplished by both magnetic and solar compasses. Thirty two paleomagnetic sites were sampled on a continuous Eocene stratigraphic section (sections C and D in Fig. 2, Fig. 4, Table 1) that covers about 185 m and corresponds to the upper lacustrine and ephemeral fluvial section of the unit (FA8). Six additional sites belong to a section located at about 1.5 km along strike (section E in Fig. 2, Fig. 4, Table 1) whose levels are stratigraphically correlated to the upper part of the main section (Melchor et al., 2006). In addition to sites that belong to the sections of Fig.4 that were used for magnetostratigraphic analysis, nine more sites were sampled in the lower lacustrine section to increase the number of data for obtaining a paleomagnetic

pole. Eight of these sites are stratigraphically below the main section and a single site (D58) was sampled on a fluvial lacustrine level interbedded in the eolian section (see Fig. 3 and Table 1).

Eight paleomagnetic sites were sampled on the Upper Triassic Quebrada Santo Domingo Formation, four of them in the basalts (Fig. 3, Table 2) to compare their magnetic directions with those recorded in the Eocene rocks.

Oriented samples were cored, and one to two specimens of fresh rock 2.5 cm in diameter and 2.2 cm long were sliced from each core. Natural remanent magnetization (NRM) before and after demagnetizations were determined using a JR6 magnetometer and a 2G cryogenic magnetometer that includes a three-axis AF demagnetizer. The stability of the NRM was tested by progressive thermal or alternating field (AF) demagnetization. A blend of AF and thermal demagnetizations was also used in some samples with more than one magnetic carrier. During thermal demagnetization, the bulk susceptibility was checked after each demagnetization step to monitor the occurrence of chemical changes induced by heating. The ChRM of each specimen was determined by applying a least square line fit (Kirschvink, 1980). In addition, different techniques were carried out to identify the magnetic carriers of the samples.

4.2. Laguna Brava Formation

4.2.1. Rock magnetism

Isothermal remanent magnetization (IRM) up to 2.3 T was applied to selected samples of the Eocene sedimentary rocks to identify the minerals carrying the magnetization, by using an ASC IM-10-30 impulse magnetizer at the Universidad de Buenos Aires. Acquisition of IRM shows that all samples contain at least two magnetic

components (Fig. 6a). The lower coercivity phase is dominant (80-90% of SIRM) and was interpreted as ferrimagnetic minerals, possibly (titano)magnetites; the higher coercivity phase shows remanence coercive force ranging from 250 to 630 mT, typical of hematite.

A hysteresis loop of one Eocene sedimentary rock (Fig. 6b) reveals that a ferrimagnetic mineral is the main magnetic mineral. Thermomagnetic curves were made from one sample (Fig. 6c) and from the magnetic material previously extracted from 12 different samples (Fig. 6d) in Ar atmosphere by using a MFK1 Agico Kappabridge. To perform the extraction, samples were ground avoiding contamination using an agate mortar. Subsequently we concentrated the magnetic material using a magnet. Both curves are similar indicating that apparently a single mineral determines the main magnetic signal. The increase in susceptibility with temperature observed up to about 370° C is typical of titanomagnetite. A subdued Verwey transition is observed at low temperatures (Fig. 6c, d), whose virtual suppression might be due either to the Ti-content or to non-stoichiometry of magnetite (Moskowitz *et al.* 1998). A change in the original magnetic carrier happened during heating, since magnetic susceptibility on cooling is decreased, might indicate the oxidized (maghemitized) character of the (titano)magnetite (Fig. 6c, d). The estimated Curie temperature is not discrete, but could belong to a range of low-Ti titanomagnetites.

It is expected that the presence of hematite either in the clasts or as pigmentary cement, would be severely masked by the effects of the strongly magnetic (titano)magnetite, particularly in high field experiments. Therefore only the response of the (titano)magnetite was clearly detected in the hysteresis curves, and hematite is a very subordinate carrier of the SIRM.

4.2.2. Magnetic behaviors

The magnetic behavior of the Eocene sedimentary rocks can be described in terms of different categories. Figure 7a shows the magnetic behavior of a sample after progressive thermal demagnetization. Two components can be identified on the basis of their relative unblocking temperatures. A low-temperature component is stable between room temperature and 200-250° C and has no geological meaning. In spite of a somewhat noisy behavior, a high-temperature component is stable from 250°C up to 580°C and after this temperature the sample has an anomalous random behavior (not represented in the figure). The high-temperature stable component constitutes the dominant proportion of the total NRM and *in-situ* it has SSE declination and a medium downward inclination. The unblocked temperature at 550-580° implies that (titano)magnetite is the main magnetic carrier of the recognized component in agreement with the rock magnetic experiments.

Figure 7b is an example of behavior where both AF and thermal demagnetizations were used. After a spurious small component is removed at 150°C, a ChRM component (that *in situ* has SSE declination and a medium downward inclination) is recognized. It is noteworthy that the vector defined from 150°C up to 12 mT is statistically undistinguishable to that defined from 300°C up to 650°C, but the latter has a higher minimum angle deviation (2.3° versus 10.5°) what suggests that in many samples the AF demagnetization was somewhat better to test the NRM stability. The mixed AF/thermal demagnetizations revealed that virtually the same component is carried by both (titano)magnetites and hematite, in agreement with the rock magnetism of the sample (see Fig. 6a).

Considering the magnetic behavior as described above, a thermal demagnetization of 150° C followed by steps of AF demagnetizations was considered as

the most effective way of characterize de ChRM. Figures 7c and d show the magnetic behavior of two samples that have the same tilt correction (Table 1). The ChRM component of the sample D56-3 *in situ* has a SSW declination and a medium downward inclination and is demagnetized up to 40 mT (after this step its intensity is 12% of the total NRM and its magnetic behavior becomes erratic). The sample D54-3 has an upward inclination ChRM component with a much harder magnetic coercivity and is closely antipodal to the previous one.

4.3. Quebrada Santo Domingo Formation

The following discussion is referred exclusively to the basalt samples from Quebrada Santo Domingo Formation, as the four sites in sedimentary rocks showed random behavior to demagnetization (see Table 2).

4.3.1. Magnetic behaviors of the Upper Triassic basalts

Hysteresis loop (Fig. 8a) and the unblocked temperatures recognized in the normalized intensity decays after each thermal demagnetization step (Fig. 8b) are both consistent with hematite as the main carrier of the magnetic remanence of site D36 of the Upper Triassic basalt flows. Only thermal demagnetization was, then, applied in the samples of these sites.

Sites D36, D37 and D39 yielded reliable upward magnetic components (Table 2; Figure 8c). *In situ* a ChRM component was defined between 400°C up to 680°C with a NW declination and a medium inclination. All the samples show similar ChRM components.

From site D38 only one sample had an interpretable magnetic behavior. Figure 8d shows that two completely different components with contrasting unblocking temperature spectra can easily be recognized. *In situ* the softer component has NNE declination and upward low inclination. This component is completely removed above 580° C and therefore, its magnetic carrier can be (titano) magnetites. The harder component, carried by hematite according to its unblocking temperature, has south declination and low downward inclination. The rest of the samples of site D38 have behaved erratically. Notice that this site also shows geochemical differences respect to the other basalt sites (Fig. 5c).

Figure 8e shows the mean components of sites D36, D37 and D39 and both the softer and harder components of the sample from site D38 after their corresponding tilt corrections. The harder component of the sample from D38 is virtually antipodal of the mean direction of the other sites. The softer component is close to the other site upward components. It is interpreted that the sample of the site D38 acquired its hard component during a chron of opposite polarity to that when the soft component was recorded, but in both cases they correspond to directions of the Earth's magnetic field similar to those recorded at sites D36, D37 and D39.

5. Validation of paleomagnetic data from the Eocene sedimentary rocks

The ChRM components determined in the specimens from the Eocene sedimentary rocks were averaged for each paleomagnetic site. Before any tilt and reversal tests, Vandamme's (1994) method was applied on the virtual paleomagnetic poles (VGPs) from the site mean directions to divide stable and intermediate data. Four VGPs that belong to the sites D01, D28, D35 and D58 (Table 1) occur away from the

VGPs enclosed by the cut-off angle determined by Vandamme's method. The mean directions of these sites were not considered in the tilt and the reversal tests that were applied. The rest of the site mean directions are shown before and after their tilt corrections respectively in Figures 9a and b. These mean directions pass the tilt test proposed by Enkin (2003) with an optimal untilting at $105.3\% \pm 60.1\%$ (Fig. 9c). As the maximum value of Kappa (Fisher, 1953) is obtained virtually at 100% of untilting (Fig. 9d), it is considered that the bedding corrections were not under or over-estimated.

When all of the tilt corrected ChRM components of both polarities are analyzed, they share a common mean at 95% confidence level (McFadden and Lowes, 1981) passing a reversal test, which is evident when one of the mean directions is inverted, as the 95% confidence (α_{95}) intervals overlap (Supplement Fig. S3).

Both the tilt and reversal tests suggest that the recorded ChRM components have a primary origin. Moreover, the stratigraphic correlation of Melchor et al. (2006) between two sections separated by 1.5 km is consistent with paleomagnetic data (Fig.4). Note that D31 and D54 sites show normal polarity, while sites that are stratigraphically above them have reverse polarity (see Table 1). This means that it is possible to make a magnetostratigraphic correlation between both sections, which also suggests that the recorded ChRM components have a primary origin.

Petrographic analysis (section 3.1.), studies of rock magnetism (section 4.2.1) and remanence stability suggest that the samples show detrital magnetization carried by low Ti (titano)magnetite, martite and hematite grains. The same ChRM was recorded by both (titano)magnetites and hematite (Fig. 7b). This can be interpreted as follows: 1) the hematite component is carried by detrital hematite (formed simultaneously with detrital magnetite) or 2) the diagenesis occurred very shortly after deposition, in case the

hematite component is carried by intrastratally grown hematite (either martite or red pigment).

Inclination shallowing of the remanence is a common problem in sedimentary rocks, mainly recognized in red beds (see Tauxe et al., 2008 and references therein). To recognize if the inclinations of the sampled sites were biased by flattening, Tauxe and Kent's (2004) method was applied. These authors have recommended using this test for a number of sites of about 100, but it was successfully performed in paleomagnetic studies with smaller number of sites (i.e. Kent and Irving, 2010). Here the method was applied to all the site mean directions (including those that were out of the cut off angle) as recommended by Tauxe and Kent (2004). The bias of inclinations due to shallowing is negligible (Supplement Fig. S4) and therefore no correction for flattening was applied. This is coherent with the open packing and zeolites of sandstones from the unit (see section 3.1.) that indicate moderate burial depth and no significant compaction.

A paleomagnetic pole (PP) was obtained from the VGPs of the selected sedimentary rocks of Laguna Brava Formation, whose geographic coordinates and statistical parameters are: $N=29$, $Lon.=184.5^{\circ}E$, $Lat.=75.0^{\circ}S$, $R=27.8$, $A_{95}=5.6^{\circ}$, $K=23.7$.

5.1. Correlation with a Global Magnetostratigraphic Chart

Based on the youngest dating of the reworked tuff level found in the main section of the Laguna Brava Formation and the different polarities recorded in it, a magnetostratigraphic correlation with the global magnetostratigraphic time scale of Cande and Kent (1995) was performed. The magnetostratigraphic correlation (Fig. 10) implies that the stratigraphic succession of the main section (Fig. 4) would have been

deposited between a time a little older than 38.1 Ma and a time a little younger than 34.7 Ma.

The correlation was used to calculate the sedimentation rates for the different recorded magnetic chrons (Fig. 11). In agreement with the petrographic analysis shown in section 3.1., it was considered that the compaction of the rocks was minor. The mean sedimentation rate for the whole analyzed section was 1.4 cm per thousand years. In detail, the lower part of the section has a sedimentation rate of 1.1 cm per thousand years, followed by an increase that coincides with the presence of undulated and wavy lamination and a decrease consistent with a sector dominated by flat bedding. The highest rates are found in deposits with mud-draped surfaces and mudstone clasts at the end of C16n.

6. Discussion

According to what is mentioned in the previous section, the paleomagnetic directions recorded by the Late Eocene Laguna Brava Formation can be considered primary and not biased by shallowing (i.e. they can be regarded useful for tectonic studies). On the other hand, also the directions carried by the Upper Triassic volcanic rocks can be considered primary whereas principal component analyses indicate that sites D36, D37 and D39 have single records of high unblocking temperature ChRMs and the harder component of the sample from site D38 is almost antipodal to the mean of the other ones.

As mentioned in Section 1, Vizán et al. (2005) considered that the magnetization carried by the lithologies outcropping in Quebrada Santo Domingo (i.e., Quebrada Santo Domingo and Laguna Brava formations) had an Early Jurassic age, after

comparing their obtained pole with apparent polar wander (APW) paths proposed by Torsvik et al. (2001) and Muttoni et al. (2001). When a composed pole is calculated from the tilt-corrected directions in Table 1 and Table 2, it is again coincident with an updated Jurassic APW path (Fig. 12; Kent and Irving, 2010). The interval of confidence of the new pole overlaps with those of Early Jurassic poles of the path and has the smaller great circle distance with the pole of 190 Ma. However, this interpretation of an Early Jurassic magnetization is at odds with the Late Eocene age from a tuff from the Laguna Brava Formation (Melchor et al., submitted) and the magnetostratigraphic correlation shown above.

When the tilt-corrected mean direction of the sedimentary sites was compared with the mean direction of the Upper Triassic basalt sites, we observed that they are different at 95% of confidence level (Fig. 13) what indicates that their magnetizations could have different ages. In other words, the age of the paleomagnetic directions of sampled sedimentary rocks of the Laguna Brava Formation is not Late Triassic-Early Jurassic as previously thought, and could be much younger considering the new isotopic age and our magnetostratigraphic correlation with a global chart, what agrees with the neoichnological study of Genise et al. (2009).

The assigned Late Eocene age indicates that the upper part of the Laguna Brava Formation (Fig. 4) could be roughly coeval with the lower member of the Vinchina Formation according to the stratigraphic scheme of Cicciooli et al. (2011), a Tertiary stratigraphic unit of Sierras Pampeanas outcropping in the northwest of La Rioja Province (Tripaldi et al., 2001). However, the Eocene age of the Vinchina Formation has been recently challenged by the presence of Early Miocene zircon grains in a reworked tuff of the lower member of the unit (Collo et al., 2011). Further likely correlations can be suggested for stratigraphic units found in Puna-Cordillera Oriental

transition (see Payrola Bosio et al., 2009). All of these deposits could belong to the initial episodes of sedimentation in a foreland basin, related to the onset of the Andean deformation (Incaic Phase?) as suggested by Coughlin et al. (1998) in Sierras Pampeanas.

We compared the Laguna Brava PP with paleomagnetic data obtained in Gran Barranca locality of equivalent ages (Ré et al., 2010). The latter were used as reference data since their sampling locations are in an undeformed area of Argentina, are accurately dated and pass the reversal test. Considering the time span that covers the sampled interval of the Laguna Brava Formation according to its magnetostratigraphy, the reference pole was recalculated to include only the sites with equivalent ages of the Sarmiento Formation provided by Ré et al. (2010), after applying Vandamme's (1994) method.

There is a mismatch between Laguna Brava PP and Gran Barranca PP (Fig. 14). Using Beck's (1989) method it is possible to observe that the dipolar paleolatitudes of Laguna Brava and Gran Barranca poles are not different at 95% confidence levels (Fig. 14). The greater differences between these data are therefore related to the declinations of their mean directions. A declination difference of about 16° can be assured for Laguna Brava compared to the Gran Barranca data. This paleomagnetic evidence can be interpreted in tectonic terms (Fig. 14); the sampling locality of Laguna Brava as belonging to a structural block can have rotated about 16° clockwise along a vertical axis after about 34 Ma. If this tectonic interpretation is true, geological units that are stratigraphically below should also submit a clockwise rotation.

The magnetic data obtained from the Upper Triassic basalts are not enough to warrant that the secular variation of Earth's magnetic field was averaged out, as they come from only 4 sites. However, as noted above (Section 3.2., Fig. 5c), the site D38

belongs to a basalt flow geochemically different to the lower and upper ones and it has a hard component that is practically antipodal to those of the other sites (section 4.3.1., Fig. 8e) suggesting that the sampled outcrop involves different cooling units that were extruded at different times. A VGP (Lat. = 55.36° S, Lon. = 209.71° E, $d\phi=5.9^{\circ}$, $d\gamma=3.8^{\circ}$) was obtained with the mean direction of three sites and the harder component of the sample from D38. We tentatively assumed that this VGP was representative of the Earth's magnetic field during Late Triassic time and compared it with a mean of three reliable paleomagnetic poles of South America (Supplement Table S3). It is evident that Late Triassic paleomagnetic data of the basalts could also record a clockwise rotation of the sampling locality (Supplement Fig. S5). An analogous interpretation is obtained if the Upper Triassic basalt VGP is compared with the updated APW path of Kent and Irving (2010). Furthermore, Geuna and Escosteguy (2004) carried out a paleomagnetic study on Carboniferous rocks in the vicinity to Quebrada Santo Domingo near Las Chacritas (see Fig. 1) and obtained a PP whose geographical position would also indicate a clockwise rotation of the sampling area (Supplement Table S4: Rincón Blanco Syncline) of a magnitude similar to the Upper Triassic basalts. Hence it is interpreted that the paleomagnetic data of different stratigraphic units from the Quebrada Santo Domingo area that covers a period that extends from the Early Permian to the Eocene, recorded a clockwise rotation of the same tectonic block, with the older units showing the highest magnitudes of rotation.

6.1. The regional setting for block rotations

The rotation of this block will be analyzed expeditiously in a regional tectonic framework in order to contextualize it within a larger scale scheme. The area being discussed (Fig. 15) is between the parallels $27^{\circ} 15'$ and 32° S, where flattening of the

Nazca Plate occurs (i.e. Jordan et al., 1983). Considering the tectonic processes related to the Andean chain, Lamb (2001) divided the Bolivian orocline in three domains. Although the southern limit of the proposed southernmost domain was not well defined, Somoza et al. (1996) had previously established a pattern of rotations for the Central Andes, whose southern boundary would be approximately at 28° south. In northwestern Argentina, at about this latitude, there is a transition zone between the Puna and Sierras Pampeanas geological provinces, expressed by a strong narrowing of the high Andean chain (de Urreiztieta et al., 1996). This NE-SW transition zone has been described as the “Tucumán lineament” by Mon (1976) and different authors based on geological and paleomagnetic data have postulated that dextral-strike slip has occurred along it (Jordan et al., 1983; de Urreiztieta et al., 1996; Aubry et al., 1996). From west to east, the area here analyzed belong to a broken foreland located between the Precordillera thin-skinned fold and thrust belt and the thick-skinned Sierras Pampeanas where the Andean deformation is conditioned by the effects of Nazca plate flat subduction (i.e. Jordan et al., 1983; Ramos et al., 2002). The geometry and the style of deformation were controlled by older crustal-scale structures represented by Late Proterozoic-Early Paleozoic terrane boundaries and Late Paleozoic-Mesozoic faults (Ramos et al., 2002). Apatite fission-track data indicate deformation associated with exhumation at different geological times (Coughlin et al., 1998): Carboniferous-Permian, Early-Middle Jurassic, Late Paleocene-Middle Eocene and Late Miocene-Pliocene.

In the study area, Rossello et al. (1996), Ré et al. (2001) and Japas and Ré (2006) defined two major associations of lineaments with NNE and NNW respective trends (Fig. 15). On the other hand, Gripp and Gordon (1990) using a global plate motion model determined absolute drifts for both the Nazca and the South America plates at about 30°S at the longitude of the trench. The drift direction (~N80°E) is close to that

presented for the motion of Nazca plate relative to a fixed South America by Anderson et al. (2004) and the GPS velocity field for the “Andes microplate” of Brooks et al. (2003) at about the same latitude. Figure 15 shows the clockwise rotations that have been calculated on the basis of paleomagnetic data (Supplement Table S4). As suggested by Aubry et al. (1996) for the “Tucumán transition zone”, other NE, but also NNE, lineaments would have acted as dextral strike slip faults rotating clockwise the crustal blocks to accommodate the deformation caused by the stress oblique to the fault trends (see also Japas and Ré, 2006). The NNW lineaments should have acted as left-lateral strike slip faults, as indicated by Introcaso and Ruiz (2001), who showed that the depocenters of the Bermejo and Ischigualasto-Villa Unión Cenozoic basins lie on opposite sides of the large NNW Desaguadero-Bermejo fault (VFFZ, Valle Fértil Fault Zone in Fig. 15), showing a left lateral offset of about 70 km. Recently, the NNW Rodeo-Talacasto sinistral transpressional belt was recognized based on *en-échelon* arrangement of a set of thrust-controlled exposures of synorogenic Tertiary rocks and the located counterclockwise deflection of both, Andean and Paleozoic structures (Japas et al., 2011). Moreover, along this NNW belt the regional nearly homogeneous clockwise block rotation pattern show rotation nulls (Japas and Ré, 2012).

The variable magnitude of the rotations could be due to different reasons: 1) structural heterogeneities present in some places that could cause different values of rotations between sites a few tens of kilometers away (Aubry et al., 1996; Japas and Ré, 2012); 2) deformation partitioning (Siame et al., 2005) and/or 3) superposed deformation processes at different geological times, each one represented by a particular intensity and remote stress field. In any case, Tertiary rotations should be completed before the deposition of the unrotated Toro Negro Formation (see Supplement Table S4) which has been dated recently by Ciccioli et al. (2005) at 8.6 and 6.8 Ma. A

significant episode of block rotations may have occurred sometime during the Late Miocene-Pliocene deformation reported by Coughlin et al. (1998), that could be roughly correlated with the earlier 6 Ma uplift stage of the Aconquija range located to the east (see Strecker et al., 1989; Ramos et al., 2002).

The discussion above makes clear that the region near the boundary of Puna-Precordillera-Sierras Pampeanas geological provinces is prone to be affected by block rotations around vertical axes, related to frequent reactivation of old crustal-scale structures. Therefore, paleomagnetic data from this area should not be used in any apparent polar wander path of South America or to test the timing of accretion of allochthonous terranes to South America in ancient times. This problem is greater the older the rocks are, considering that several deformations occurred from the Carboniferous till the Pliocene and that the direction of convergence of Nazca or other Pacific plates to South America could have changed over time (see for example Pardo Casas and Molnar, 1987 or Somoza and Ghidella, 2005). Then it becomes extremely difficult to determine if a block had different senses of rotation caused by different tectonic events at different times. For instance, if the Early Cambrian paleomagnetic pole of Cerro Totorá (Rapalini and Astini, 1998) is compared with the mean Early Cambrian pole for Gondwana of McElhinny and McFadden (2000), its anomalous position could be explained simply as a counterclockwise block rotation of about 15° instead as an evidence that Precordillera was part of Laurentia in Early Cambrian time (Supplement Fig. S6). Cerro Totorá, located at $29^\circ 30' S$ and $68^\circ 40' W$, is not far from the VFFZ (Fig. 15), a structure that could be periodically activated since at least the Paleozoic.

7. Conclusions

A primary magnetization carried by (titano)magnetite (plus hematite) in detrital grains, was isolated from samples of Eocene red beds of the Laguna Brava Formation. The magnetization passes both tilt and reversal tests, and it does not seem to be affected by inclination-shallowing.

The sequence, previously thought to be Late Triassic-Early Jurassic in age, has been dated recently as Late Eocene. A magnetostratigraphic correlation was possible between two sections in the same locality. The correlation with a global magnetostratigraphic chart allowed establishing that the main sampled sequence was deposited during the Late Eocene, with a mean sedimentation rate of about 1.4 cm per thousand years, probably as the Andean synorogenic fill of a foreland basin.

When compared to Eocene poles of stable South America, the Laguna Brava pole seems to be rotated clockwise about 16° , in a way consistent with other rotations detected in the region.

The match of the unrotated pole with the Early Jurassic APWP for South America and the lack of radiometric dating (made available only recently) had led to the misinterpretation of preliminary paleomagnetic data.

The new paleomagnetic and radiometric data of the rocks of Quebrada Santo Domingo led to a coherent interpretation within a regional tectonic and stratigraphic framework. It turns to be an excellent example of how easy can be to misunderstand paleomagnetic data, and reinforces the need of supporting them with a thorough comprehension of the regional geological framework, and with additional techniques such as radiometric dating, and petrographical, mineralogical and geochemical examination of the sampled rocks.

The consistency of this interpretation is fundamental to solve the conundrum stated in the introduction of this paper. The age of the succession containing the bird

footprints reported by Melchor et al. (2002) is Late Eocene and is, therefore, consistent that the avian footprints found in them belong to birds with behaviors similar to extant sandpipers.

Acknowledgments

This work was partially supported by grants from: Universidad de Buenos Aires (H.V., UBACyT 20020100100894, UBACyT 20020110100064), Agencia Nacional de Promoción Científica y Tecnológica (S.G., PICT-2011-0956) and Consejo Nacional de Investigaciones Científicas y Tecnológicas (H.V., PIP 112-200801-02828, S.G., PIP 112-200801-01502).

References

- Anderson, M.L., Zandt, G., Triep, E., Fouch, M., Beck, S., 2004. Anisotropy and mantle flow in the Chile-Argentina subduction zone from shear wave splitting analysis. *Geophysical Research Letters* 31, L23608, doi:10.1029/2004GL020906.
- Arcucci, A., Marsicano, C., Coria, R.A., 2005. Una nueva localidad fosilífera en el Cretácico de la Precordillera de La Rioja. *Ameghiniana* 42, 60R.
- Artabe, A. E., Brea, M., Zamuner, A.B., 1999. *Rhexoxylon bruni* Artabe, Brea et Zamuner, sp. nov., a new Corystosperm from the Paramillo de Uspallata, Mendoza, Argentina. *Review of Palaeobotany and Palynology* 105, 63-74.
- Atkins, J.E., McBride, E.F., 1992. Porosity and packing of Holocene river, dune, and beach sands. *American Association of Petroleum Geologists Bulletin* 76, 339-355.
- Aubry, L., Roperch, P., de Urreiztieta, M., Rosello, E., Chauvin, A., 1996. Paleomagnetic study along the southeastern edge of the Altiplano - Puna

- Plateau: Neogene tectonic rotations. *Journal of Geophysical Research* 101, b8, 17,883-17,899.
- Beck, M.E. Jr, 1989. Block rotations in continental crust: examples from western North America, in: Kissel, C., Laj, C. (Eds.), *Paleomagnetic rotations and continental deformation*. Nato ASI Series, Series C: Mathematical and Physical Sciences 254, Kluwer Academic Publishers, Dordrecht, pp. 1-16.
- Bish, D.L., Boak, J.M., 2001. Clinoptilolite-haundite nomenclature., in: Bish, D. and Ming, D. (Eds.), *Natural zeolites: occurrence, properties, applications*. Mineralogical Society of America, *Reviews in Mineralogy* 45, Michigan, pp. 207-216.
- Boles, J.R., Surdam, R.C., 1979. Diagenesis of volcanogenic sediments in a Tertiary saline lake; Wagon Bed Formation, Wyoming. *American Journal of Science* 279, 832-853.
- Brooks, B.A., Bevis, M., Smalley, R., Kendrick, E., Manceda, R., Lauría, E., Maturana, R., Araujo, M., 2003. Crustal motion in the Southern Andes (26° –36° S): Do the Andes behave like a microplate? *Geochemistry Geophysics Geosystems* 4, 101085, doi:10.1029/2003GC000505.
- Camino, R., Fauqué, L., 2001. Hoja geológica 2969-II, Tinogasta. Provincias de La Rioja y Catamarca. Instituto de Geología y Recursos Minerales, Servicio Geológico Minero Argentino, Boletín 276, Buenos Aires.
- Camino, R., Zamuner, A.B., Limarino, C.O., Fauqué, L., 1995. El Triásico superior fosilífero en la Precordillera riojana. *Revista de la Asociación Geológica Argentina* 50, 262-265.

- Cande, S.C., Kent, D.V., 1995. Revised calibration of the geomagnetic polarity timescale for the Late Cretaceous and Cenozoic. *Journal of Geophysical Research* 100, 6093-6095.
- Chipera, S.J., Apps, J.A., 2001. Geochemical stability of natural zeolites, in: Bish, D. and Ming, D. (Eds.), *Natural zeolites: occurrence, properties, applications*. Mineralogical Society of America, *Reviews in Mineralogy* 45, Michigan, pp. 117-143.
- Ciccioli, P.L., Limarino, C.O., Marensi, S.A., 2005. Nuevas edades radimétricas para la Formación Toro Negro en la Sierra de los Colorados, Sierras Pampeanas Noroccidentales, prov. la Rioja. *Revista de la Asociación Geológica Argentina* 60(1), 251-254.
- Ciccioli, P.L., Limarino, C.O., Marensi, S.A., Tedesco, A.M., Tripaldi, A., 2011. Tectosedimentary evolution of the La Troya and Vinchina depocenters (northern Bermejo Basin, Tertiary), La Rioja, Argentina, in: Salfity, J.A., Marquillas, R.A. (Eds.), *Cenozoic Geology of the Central Andes of Argentina*. SCS Publisher, Salta, pp. 91-110.
- Collo, G., Dávila, F.M., Nóbile, J., Astini, R.A., Gehrels, G., 2011. Clay mineralogy and thermal history of the Neogene Vinchina Basin, central Andes of Argentina: Analysis of factors controlling the heating conditions. *Tectonics* 30, TC4012.
- Coughlin, T.J., 2000. *Linked Orogen-Oblique Fault Zones in the Central Andes: The Basis of a New Model for Andean Orogenesis and Metallogensis*. Ph D. thesis University of Queensland, Brisbane, 157 pp.
- Coughlin, T.J., O'Sullivan, P.B., Kohn, B.P., Holcombe, R.J., 1998. Apatite fission-track thermochronology of the Sierras Pampeanas, central western Argentina:

- Implications for the mechanism of plateau uplift in the Andes. *Geology* 26(11), 999-1002.
- de Urreiztieta, M., Gapais, D., Le Corre, C., Cobbold, P.R., Rossello, E., 1996. Cenozoic dextral transpression and basin development at the southern edge of the Puna Plateau, northwestern Argentina. *Tectonophysics* 245, 17-39.
- de Valais, S., Melchor, R.N., 2008. Ichnotaxonomy of bird-like footprints: An example from the Late Triassic-Early Jurassic of northwest Argentina. *Journal of Vertebrate Paleontology* 28, 145–159.
- Enkin, R.J., 2003. The direction-correction tilt test: An all-purpose tilt/fold test for paleomagnetic studies. *Earth and Planetary Science Letters* 212, 51-166.
- Fisher, R.A., 1953. Dispersion on a sphere. *Proceedings of the Royal Society of London, Series A* 217, 295-305.
- Folk, R.L., Andrews, P.B., Lewis, D.W., 1970. Detrital sedimentary rock classification and nomenclature for use in New Zealand. *New Zealand Journal of Geology and Geophysics* 13, 937-968.
- Garrone, A.L., Dávila, F.M., Astini, R.A., 2008. Definición de la Formación Laguna Brava (Cretácico?): Estratigrafía, paleoambientes y correlación, 17 Congreso Geológico Argentino, Actas, 111-112.
- Genise, J.F., Melchor, R.N., Archangelsky, M., Bala, L.O., Straneck, R., de Valais, S., 2009. Application of neoichnological studies to behavioural and taphonomic interpretation of fossil bird-like tracks from lacustrine settings: The Late Triassic–Early Jurassic? Santo Domingo Formation, Argentina. *Palaeogeography, Palaeoclimatology, Palaeoecology* 272, 143–161.

- Geuna, S.E., Escosteguy, L.D., 2004. Palaeomagnetism of the Upper Carboniferous–Lower Permian transition from Paganzo basin, Argentina. *Geophysical Journal International* 157, 1071–1089.
- Gradstein, F.M., Ogg, J.G., Smith, A.G., Bleeker, W., Lourens, L.J., 2004. A new Geologic Time Scale, with special reference to Precambrian and Neogene. *Episodes* 27, 83-100.
- Gripp, A., Gordon, R., 1990. Current plate velocities relative to the hotspots incorporating the Nuvel-1 global plate motion model. *Geophysical Research Letters* 17(8), 1109-1112.
- Hay, R.L., Sheppard, R.A., 2001. Occurrence of Zeolites in sedimentary rocks: An Overview, in: Bish, D. and Ming, D. (Eds.): *Natural zeolites: occurrence, properties, applications*. Mineralogical Society of America, *Reviews in Mineralogy* 45, Michigan, pp. 217-234.
- Harrell, J., 1984. A visual comparator for degree of sorting in thin and plane sections. *Journal of Sedimentary Petrology* 54, 646-650.
- Iijima, A., 1988. Diagenetic transformations of minerals as exemplified by zeolites and silica minerals-A japanese view, in: Chilingarian, G.V., Wolf, K.H. (Eds.), *Developments in Sedimentology*. Elsevier, pp. 147-211.
- Iijima, A., Utada, M., 1966. Zeolites in sedimentary rocks, with reference to the depositional environments and zonal distribution. *Sedimentology* 7, 327-357.
- Introcaso, A., Ruiz, F., 2001. Geophysical indicators of Neogene strike-slip faulting in the Desaguadero-Bermejo tectonic lineament (northwestern Argentina). *Journal of South America Earth Sciences* 14, 655-663.

- Japas, M.S., Ré, G. H., 2006. Deformación heterogénea y rotación según ejes verticales: dos ejemplos de los Andes Centrales de Argentina. Asociación Geológica Argentina. Serie D: Publicación Especial No. 6, 99-106.
- Japas, M.S., Ré, G.H., 2012. Neogene tectonic block rotations and margin curvature at the Pampean flat slab segment (28 – 33 SL, Argentina). *Geacta* 37 (1), 1-2.
- Japas, M.S., Ré, G.H., Vilas, J.F., Oriolo, S., 2011. Oblique megashear zones in the Precordillera (Central Andes, Argentina): The Rodeo-Talacasto transpressional belt. Deformation, Rheology and Tectonics (DRT Meeting), Abstract, Oviedo, Spain.
- Jordan, T.E., Isaks, B.L., Allmendinger, R.W., Brewer, J.A., Ramos, V.A., Ando, C.J., 1983. Andean tectonics related to geometry of subducted Nazca plate. *Geological Society of America Bulletin* 94(3), 341-361.
- Kent, D.V., Irving, E., 2010. Influence of inclination error in sedimentary rocks on the Triassic and Jurassic APW path for North America and implications for Cordilleran Tectonics. *Journal of Geophysical Research* 115, B10103, doi:10.1029/2009JB007205.
- Kirschvink, J.L., 1980. The least square line and plane and the analysis of paleomagnetic data. *Journal of the Royal Astronomical Society* 62, 699-718.
- Lamb, S., 2001. Vertical axis rotation in the Bolivian orocline, South America. 1. Paleomagnetic analysis of Cretaceous and Cenozoic rocks. *Journal of Geophysical Research* 106, No. B11, 26,605-26,630.
- McBride, E.F., Diggs, T.N., Wilson, J.C., 1991. Compaction of Wilcox and Carrizo sandstones (Paleocene-Eocene) to 4420 M, Texas Gulf Coast. *Journal of Sedimentary Research* 61, 73-85.

- McElhinny, M.W., McFadden, P.L., 2000. Paleomagnetism (continents and oceans). Academic Press, USA, 382 p.
- McFadden, P.L., Lowes, F.J., 1981. The discrimination of mean directions drawn from Fisher distributions. *Geophysical Journal of the Royal Astronomical Society* 67, 19-33.
- Melchor, R.N., de Valais, S., Genise, J.F., 2002. Bird-like fossil footprints from Late Triassic. *Nature* 417, 936-938.
- Melchor, R.N., Bedatou, E., de Valais, S., Genise, J.F., 2006. Lithofacies distribution of invertebrate and vertebrate trace-fossil assemblages in an Early Mesozoic ephemeral fluvio-lacustrine system from Argentina: Implications for the *Scoyenia* ichnofacies. *Palaeogeography, Palaeoclimatology, Palaeocology* 239, 253-285.
- Melchor, R.N., Buchwaldt, R., Bowring, S.A., submitted. Supposed Late Triassic bird tracks are Eocene. *Nature*.
- Meschede, M., 1986. A method of discriminating between different types of mid-oceanic ridge basalts and continental tholeiites with the Nb-Zr-Y diagram. *Chemical Geology* 56, 207-218.
- Mon, R., 1976. La Tectónica del borde oriental de los Andes en las provincias de Salta, Tucumán y Catamarca, República Argentina. *Revista de la Asociación Geológica Argentina* 31(1), 65-72.
- Moore, D. M., Reynolds Jr., R.C., 1989. X-ray Diffraction and the Identification and Analysis of Clay Minerals. Oxford University Press, Oxford.
- Moskowitz, B.M., Jackson, M., Kissel, C., 1998. Low-temperature magnetic behavior of titanomagnetites. *Earth and Planetary Science Letters* 157, 141-149.

- Muttoni, G., Garzanti, E., Alfonsi, L., Cirilli, S., Germani, D., Lowrie, W., 2001. Motion of Africa and Adria since the Permian: paleomagnetic and paleoclimatic constraints from northern Libya. *Earth and Planetary Science Letters* 192, 159-174.
- Pardo-Casas, F., Molnar, P., 1987. Relative motion of the Nazca (Farallon) and South American plates since late Cretaceous time. *Tectonics* 6(3), 233-248.
- Payrola Bosio, P., Powell, J., del Papa, C., Hongn, F., 2009. Middle Eocene deformation–sedimentation in the Luracatao Valley: Tracking the beginning of the foreland basin of northwestern Argentina. *Journal of South American Earth Sciences* 28, 142–154.
- Pittman, E.D., Larese, R.E., 1991. Compaction of lithic sands: experimental results and applications. *American Association of Petroleum Geologists Bulletin* 75, 1279-1299.
- Ramos, V.A., Cristallini, E., Pérez, D., 2002. The Pampean flat – slab of the Central Andes. *Journal of South American Earth Sciences* 15, 59-78.
- Rapalini, A.E., Astini, R.A., 1998. Paleomagnetic confirmation of the Laurentian origin of the Argentine Precordillera. *Earth and Planetary Science Letters* 155, 1-14.
- Ré, G., Japas, M.S., Barredo, S.P., 2001. Análisis de fábrica deformacional (AFD): El concepto fractal cualitativo aplicado a la definición de lineamientos cinemáticos ándicos en el noroeste y centro-oeste argentino. *Asociación Geológica Argentina, Serie D: Publicación Especial N°5*, 75-82.
- Ré, G., Geuna, S.E., Vilas, J.F., 2010. Paleomagnetism and magnetostratigraphy of Sarmiento Formation (Eocene-Miocene) at Gran Barranca, Chubut, Argentina, in: Madden, R.H., Carlini, A.A., Vucetich, M.G., Kay, R.F. (Eds.), *The*

- Paleontology of Gran Barranca: Evolution and Environmental Change through the Middle Cenozoic of Patagonia. Cambridge University Press, pp. 32-45.
- Rossello, E. A., Mozetic, M.E., Cobbold, P.R., de Urreiztieta, M., Gapais, D., 1996. El espolón Umango-Maz y la conjugación sintaxial de los Lineamientos Tucumán y Valle Fértil (La Rioja, Argentina). Actas XIII Congreso Geológico Argentino y III Congreso de Exploración de Hidrocarburos, I, 453-471. Buenos Aires.
- Siame, L.L., Bellier, O., Sébrier, M., Araujo, M., 2005. Deformation partitioning in flat slab subduction setting: Case of the Andean foreland of western Argentina (28 S-33 S). *Tectonics* 24, TC5003, 24p.
- Somoza R., Ghidella, M., 2005. Convergencia en el margen occidental de América del Sur durante el Cenozoico: subducción de las placas de Nazca, Farallón y Aluk. *Revista de la Asociación Geológica Argentina* 60 (4), 797-809.
- Somoza, R., Singer, S., Coira, B., 1996. Paleomagnetism of upper Miocene ignimbrites at the Puna: An analysis of vertical axis rotations in the central Andes. *Journal of Geophysical Research* 101, 11,387-11,400.
- Strecker, M.R., Cervený, P., Bloom, A.L., Malizia, D., 1989. Late Cenozoic tectonism and landscape development in the foreland of the Andes: Northern Sierras Pampeanas (26-27S), Argentina. *Tectonics* 8, 517-534.
- Surdam, R.C., Sheppard, R.A., 1978. Zeolites in saline, alkaline-lake deposits, in: L.B. Sand and F.A. Humpton (Eds.), *Natural zeolites occurrence, properties, use*, Pergamon Press.
- Tauxe, L., Kent, D.V., 2004. A simplified model for the geomagnetic field and the detection of shallow bias in paleomagnetic inclinations: Was the ancient magnetic field dipolar? In: Channell, J.E.T., Kent, D.V., Lowrie, W., Meert, J.G.

- (Eds.), Timescales of the Paleomagnetic Field. Geophysical Monograph Series, American Geophysical Union 145, pp. 101-115.
- Tauxe, L., Kodama, K.P., Kent, D.V., 2008. Testing corrections for paleomagnetic inclination error in sedimentary rocks: A comparative approach. *Physics of the Earth and Planetary Interiors* 169, 152-165.
- Taylor, J.M., 1950. Pore space reduction in sandstones. *American Association of Petroleum Geologists Bulletin* 34, 710-716.
- Torsvik, T.H., Van der Voo, R., Meert, J.G., Mosar, J., Walderhaug, H.J., 2001. Reconstructions of the continents around the North Atlantic at about the 60th parallel. *Earth and Planetary Science Letters* 187, 55–69.
- Tripaldi, A., Net, L., Limarino, C.O., Marensi, S., Ré, G., Caselli, A., 2001. Paleoambientes sedimentarios y procedencia de la Formación Vinchina, Mioceno, noroeste de la provincia de La Rioja. *Revista de la Asociación Geológica Argentina* 56(4), 443-465.
- Vandamme, D., 1994. A new method to determine paleosecular variation. *Physics of the Earth and Planetary Interiors* 85, 131-142.
- Vizán, H., Geuna, S., Melchor, R.N., Bellosi, E.S., Genise, J.F., 2005. Preliminary paleomagnetic data from the Santo Domingo Formation (La Rioja, NW Argentina): geochronologic and tectonic implications. 16° Congreso Geológico Argentino, Actas, pp. 223-226.
- Wilkin, R.T., Barnes, H.L., 1998. Solubility and stability of zeolites in aqueous solution: I. Analcime, Na-, and K-clinoptilolite. *American Mineralogist* 83, 746-761.

Wilson, J.C., McBride, E.F., 1988. Compaction and porosity evolution of Pliocene sandstones, Ventura Basin, California American Association of Petroleum Geologists Bulletin 72, 664-681.

Winchester, J.A., Floyd, P.A., 1977. Geochemical discrimination of different magma series and their differentiation products using immobile elements. Chemical Geology 20, 325-343.

Figure captions

Fig. 1. Simplified geologic map of the study area. Modified from Caminos and Fauqué (2001).

Fig. 2. Detailed geologic map of the Quebrada Santo Domingo red bed succession, distinguishing between the Quebrada Santo Domingo and Laguna Brava formations. Location of measured sections, geological structures, sites of radiometric dating and fossil findings are indicated.

Fig. 3. Schematic section for the Quebrada Santo Domingo and Laguna Brava formations (sections A to F in Fig. 2). Recognized facies associations (FA1 to FA9) and location of paleomagnetic sites are also indicated.

Fig. 4. Detailed sedimentologic log of the upper lacustrine and ephemeral fluvial section (FA 8) of the Laguna Brava Formation with location of paleomagnetic sites and samples for petrographic studies. Modified after Melchor et al. (2006)

Fig. 5. Geochemical data for basalt lava flows of the Quebrada Santo Domingo Formation (see location of samples in Fig. 3).

Fig. 6. Rock magnetic analysis of representative Eocene samples. a) IRM: Acquisition of isothermal remanent magnetization for selected specimens. Although SIRM is dominated by a low-coercive phase (magnetite s.l.), a fraction of about 10-20% of SIRM is carried by a highly coercive phase which starts to saturate above 100 mT. b)

Hysteresis loop of sample from site D08. c) and d) Low-field thermomagnetic curves, applied field 200 A/m; heating/cooling as full/dashed line, respectively. c) Sample from site D25; d) concentrated magnetic material from 12 samples.

Fig. 7. Orthogonal plot of progressive demagnetization data of the Eocene sedimentary rocks. a) Thermal demagnetization. b) Combination of thermal and alternative field demagnetizations (see text for further details). c) and d) Alternative field demagnetization with a first step of thermal demagnetization of 150°C, notice that the characteristic remanent magnetizations correspond to opposite polarities.

Fig. 8. a) Hysteresis loop of an Upper Triassic basalt sample of site D36. b) Normalized intensity decays after thermal steps of demagnetization of a basalt sample of site D36. c) Orthogonal plot of progressive demagnetization data of a basalt sample of site D36. e) Basalt sample of site D38: stereographic projection, normalized decays after steps of thermal demagnetization and orthogonal plot of progressive demagnetization data. f) Stereographic projection of directions of basalt flows after tilt corrections.

Fig. 9. a) and b) Stereographic projection of site-level mean characteristic remanent magnetization directions of Eocene samples (Laguna Brava Formation). a) *in situ* coordinates. b) tilt corrected coordinates. c) tilt test and its statistical parameters (Enkin, 2003) for Eocene mean directions. d) Statistical parameter Kappa values vs. percentage of untilting for the Eocene mean directions.

Fig. 10. Magnetostratigraphic correlation of the main section of Laguna Brava Formation analyzed in this paper with a global magnetic scale (Cande and Kent, 1995).

Latitude of the VGPs after rotating them counterclockwise 16° (see Section 6. and Fig. 14). Paleomagnetic sites as in Fig. 4.

Fig. 11. Sedimentation rates of the upper lacustrine and ephemeral fluvial section of the Laguna Brava Formation obtained according to the magnetostratigraphic correlation of the local column with the global polarity time scale of Cande and Kent (1995).

Fig. 12. Composite apparent polar wander path of Kent and Irving (2010) and a paleomagnetic pole (ELT) using both Eocene and Late Triassic data together, in South America geographic coordinates.

Fig. 13. Stereographic projection of tilt-corrected site-level mean directions of Eocene samples and tilt-corrected site-level mean directions of Upper Triassic basalt samples (including the hard component of sample D38).

Fig. 14. Comparison of the paleomagnetic pole of the Eocene rocks (before and after its restoration applying a counterclockwise rotation around a vertical axis in its sampling site) with the pole of Gran Barranca locality (recalculated with data of Gran Barranca and Vera members of Sarmiento Formation). Arrows indicate the interpretation of a tectonic rotation. SD: Quebrada Santo Domingo, LB: Laguna Brava, GB: Gran Barranca.

Fig. 15. Structural map between parallels 28° S and 33° S and meridians 62° W and 71° W with the main lineaments regionally recognized. The angles between the north-south direction and the small arrows indicate the rotation of different crustal blocks (see

Supplement Table S4). The great arrow points out the direction of convergence of South America and Nazca plates. VFFZ: Valle Fértil Fault Zone. TFZ: Tucumán Fault Zone. An: Antofalla, LP-CG: La Poma-Cerro Galán, SC-PAN: Santa Clara-Paso Agua Negra, U-C: Uspallata-Catamarca, BLPB: Barreal Las Peñas Belt, RTB: Rodeo Talacasto Belt, Ch-Ch: Chilecito-Chepes, CR-DF: Cerro Rincón-Dean Funes.

Table 1. Data for calculation of paleomagnetic pole and magnetostratigraphy of the Laguna Brava Formation (location of paleomagnetic sites in Fig. 4)

Site	N/n	In Situ		Strike (°)	Dip (°)	Paleohorizontal		α_{95}	k	VGP	
		Declination (°)	Inclination (°)			Declination (°)	Inclination (°)			Lon.	Lat.
*D01	3/2	135.5	60.0	16	12	151.2	52.6			3.3	- 64.9
D02	3/3	200.7	48.4	16	12	187.2	48.0	15.6	64	207.8	- 83.7
D08	4/4	358.8	15.1	232	22	357.4	-2.8	10.2	82	285.6	62.8
D03	4/4	202.5	34	200	3	204.5	33.8	5.8	252	182.6	- 65.5
D11	3/0			200	3						
D09	3/0			232	22						
D12	3/3	6.9	-7.6	232	22	11.3	-22.7	8.5	209	325.8	70.2
D13	3/2	28	19.3	232	22	22.9	9.4			328.5	50.1
D10	3/3	356.8	-30.9	232	22	8.7	-47.7	17.1	53	25.4	82.4
D14	3/0			232	22						
D05	5/5	201.0	46.1	200	3	204.1	46.0	14.6	28	204.0	- 68.7
D04	4/4	181.7	57.6	200	3	186.3	58.4	7.8	141	266.7	- 78.2
D15	3/3	2.5	-36.5	198	42	35.1	-35.9	18.9	43	14.1	57.0
D16	5/5	4.0	-34.3	252	20	12.4	-52.3	9.4	67	46.7	78.5
D17-18	5/5	2.2	-24.6	252	20	7.5	-43.1	17.6	20	355.8	82.5
D20	4/4	188.8	30.8	234	14	196.3	40.1	9.1	102	183.8	- 74.3
D19	3/0			234	14						
D21	4/4	13.0	-20.7	234	14	18.2	-29.4	15	39	347.9	68.9
D22	3/0			234	14						

D23	3/0			234	14							
D24	3/3	353.9	-48.5	234	14	5.3	-60.0	26.9	22	93.4	76.9	
D25	3/3	180.8	47.9	228	10	190.0	54.7	18.3	46	242.2	-	79.2
D26	4/4	192.3	54.5	228	10	205.8	59.4	8.6	115	237.0	-	65.8
D27	5/3	184.6	-12	228	10	183.5	-5.1	15	71	118.0	-	58.7
*D28	4/4	334.4	-70.1	228	10	349.3	-79.3	17.7	28	117.0	48.7	
D29	3/0			228	10							
D30	3/0			228	10							
D31	4/3	353.1	-7.1	228	10	355.1	-15.1	9.8	160	277.8	68.7	
D32	3/3	183.8	52.0	228	10	195.1	58.3	6.2	399	245.2	-	73.7
D33	3/2	184.1	16.5	228	10	186.8	23.3			133.8	-	72.4
D34	3/3	201.7	60.8	228	10	220.0	63.8	25.1	25	240.6	-	54.3
*D35	8/7	129.2	45.9	228	10	127.1	55.8	15.1	17	257.1	-	45.2
D54	7/7	30.7	-40.9	200	3	33.2	-40.3	7.6	65	18.5	59.7	
D53	3/0			220	4							
D52	5/4	182.7	28.2	220	4	184.5	30.6	10.9	72	131.2	-	77.3
D55	3/2	205.3	33.6	200	3	207.3	33.3			184.8	-	63.0
D56	3/3	207.4	41.5	200	3	210.0	41.0	15.1	67	197.7	-	62.6
D57	3/3	201.1	38.5	200	3	203.5	38.4	15.7	62	188.6	-	67.7

Additional Data for Paleomagnetic Pole

D06	4/0			220	134							
D44	3/0			232	39							

D49	3/3	167.9	18.6	232	39	183.9	51.7	21.1	35	250.9	-	84.9
D48	3/0			232	39							
D47	3/0			232	39							
D45	3/0			232	39							
D46	7/7	182.1	7	232	39	193.2	34.9	8.7	49	166.6	-	74.8
D07	3/3	151.6	22.3	190	81	211.4	38.8	33	15	195.3	-	60.9
*D58	7/6	193.6	77.5	200	3	267.2	77.5	17.4	16	274.9	-	48.9

N: number of specimens that were demagnetized, n: number of specimens used in mean calculation, α_{95} : radius of the 95% cone of confidence, k: precision parameter (Fisher, 1953).

* Sites with VGPs away from the cut off angle determined by Vandamme's (1994) method.

Table 2 Paleomagnetic data for Quebrada Santo Domingo Formation

Site	N/n	In situ		Strike	Dip	Paleohorizontal		α_{95}	k
		Declination	Inclination			Declination	Inclination		
D36	3/3	343.5	-28.2	206	70	46.3	-46.1	12.6	96
D37	3/3	345.4	-20.9	206	70	36.2	-43.9	12.7	95
D38	3/1	178.0	15.6	222	65	218.8	46.05		
D39	4/4	354.0	-15.4	222	65	36.5	-49.6	10.0	85
D40	3/0			228	50				
D41	3/0			228	50				
D42	3/0			228	50				
D43	3/0			232	39				

N: number of specimens that were demagnetized, n: number of specimens used in mean calculation, α_{95} : radius of the 95% cone of confidence, k: precision parameter (Fisher, 1953).

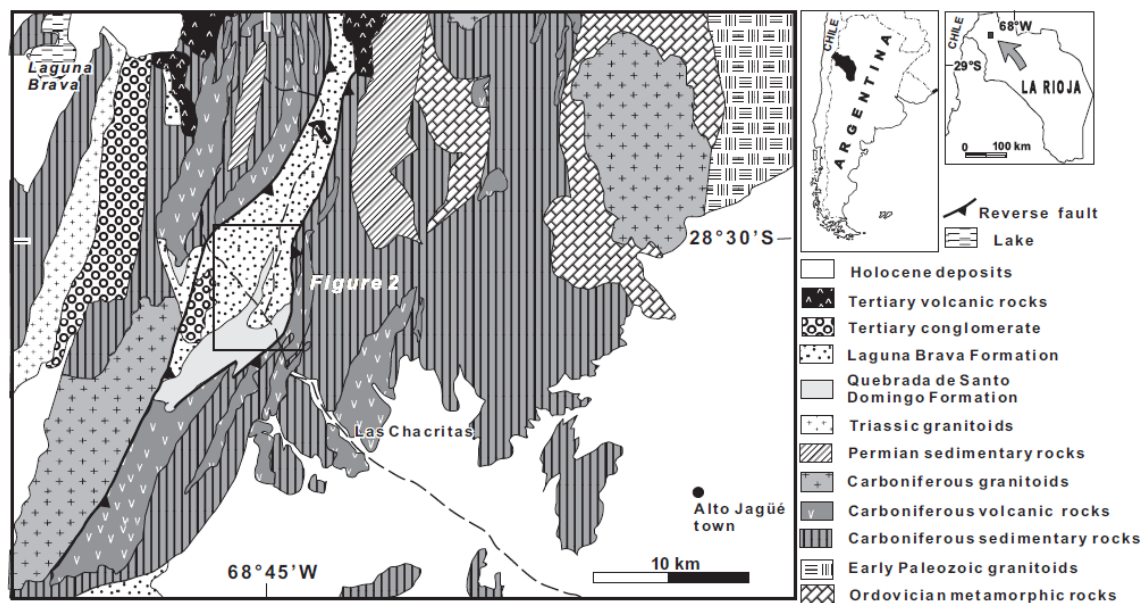


Figure 1

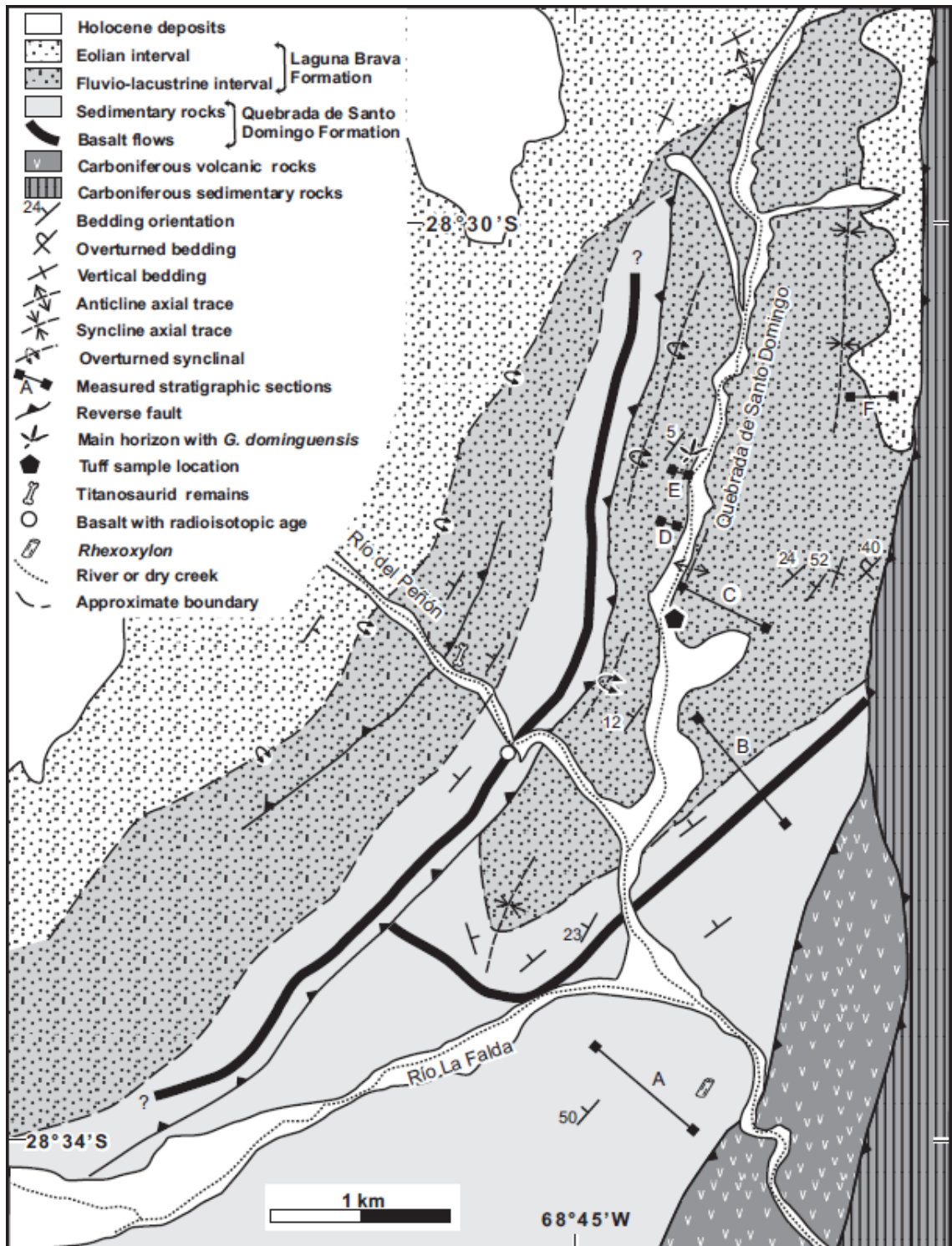


Figure 2

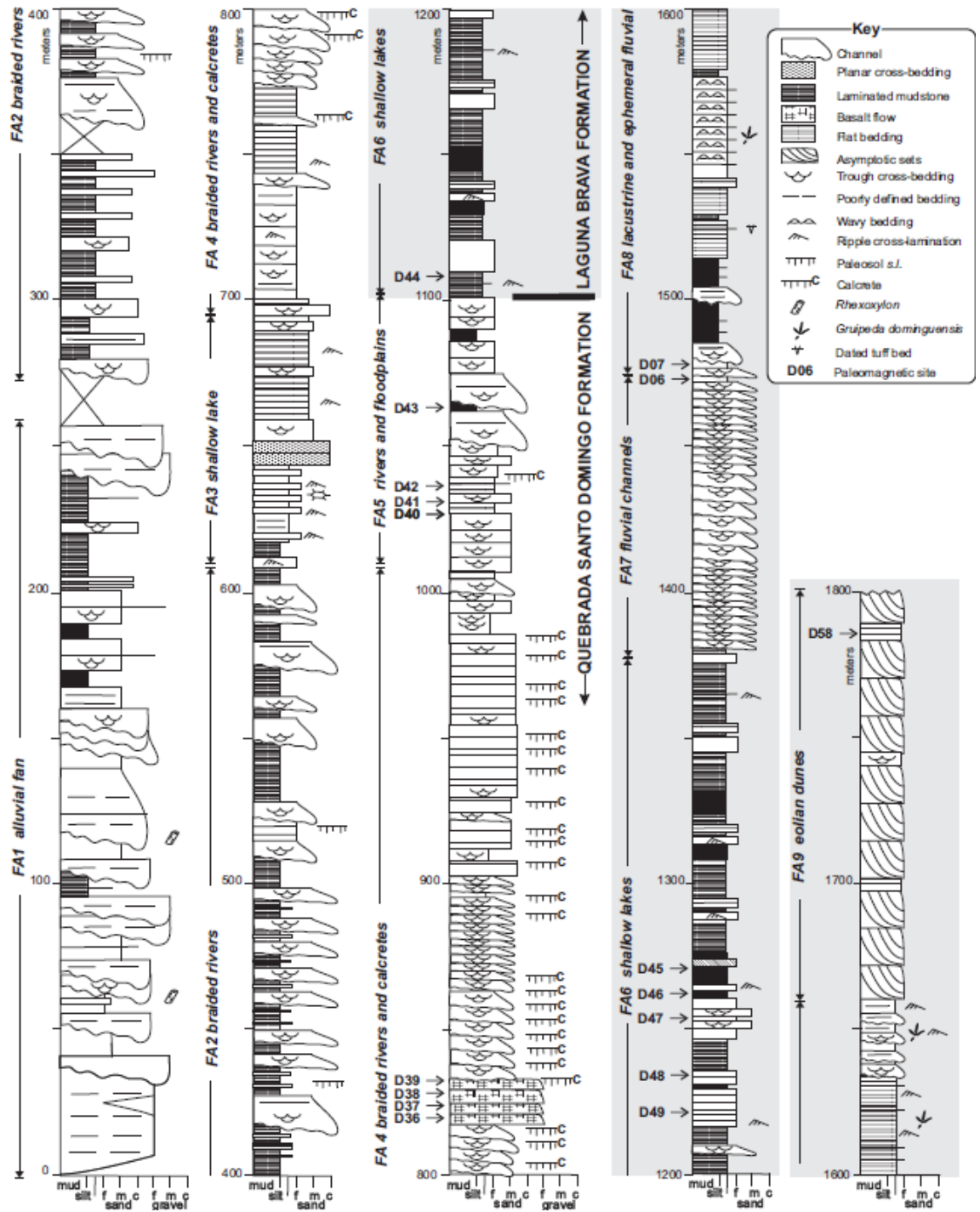


Figure 3

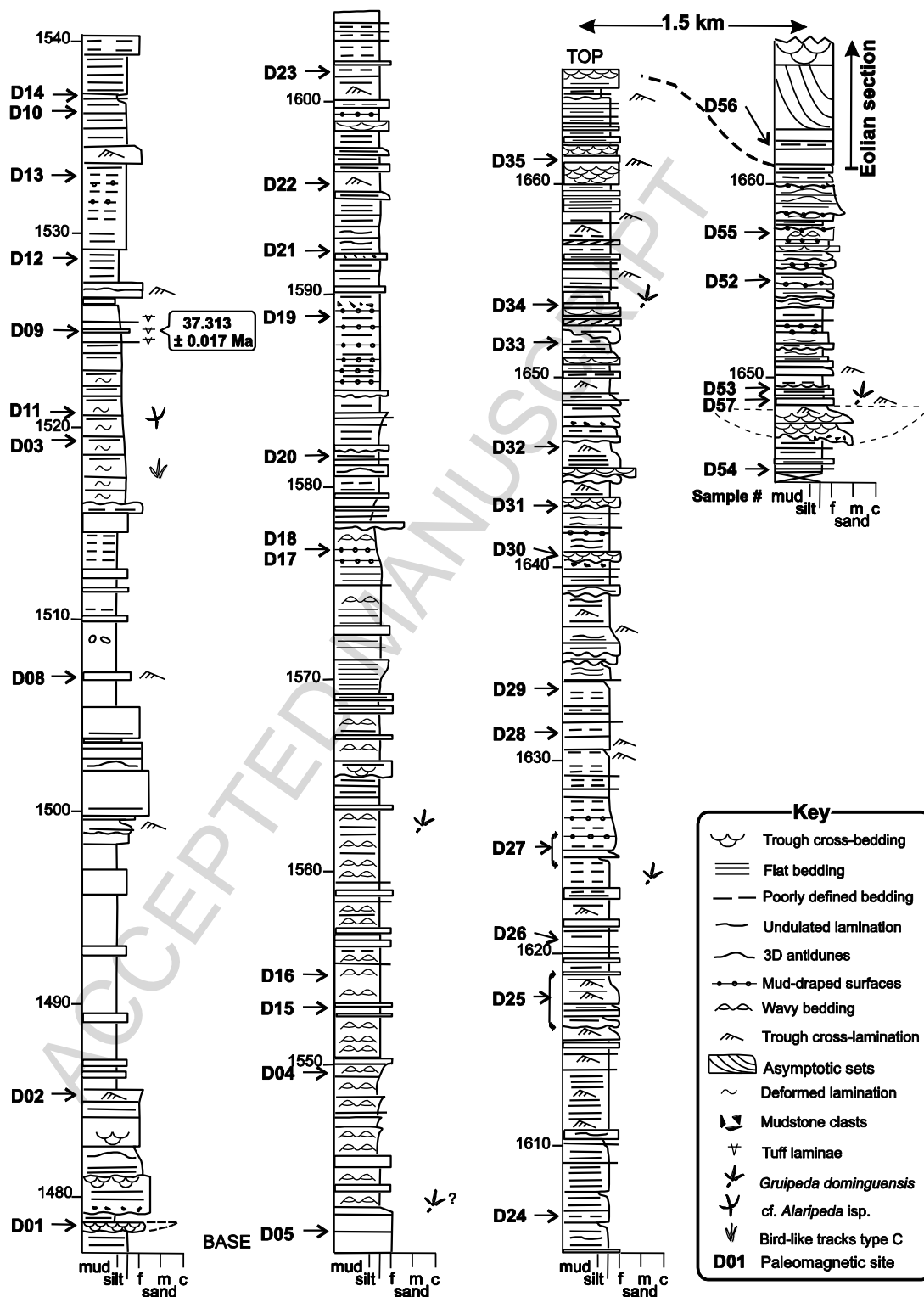


Figure 4

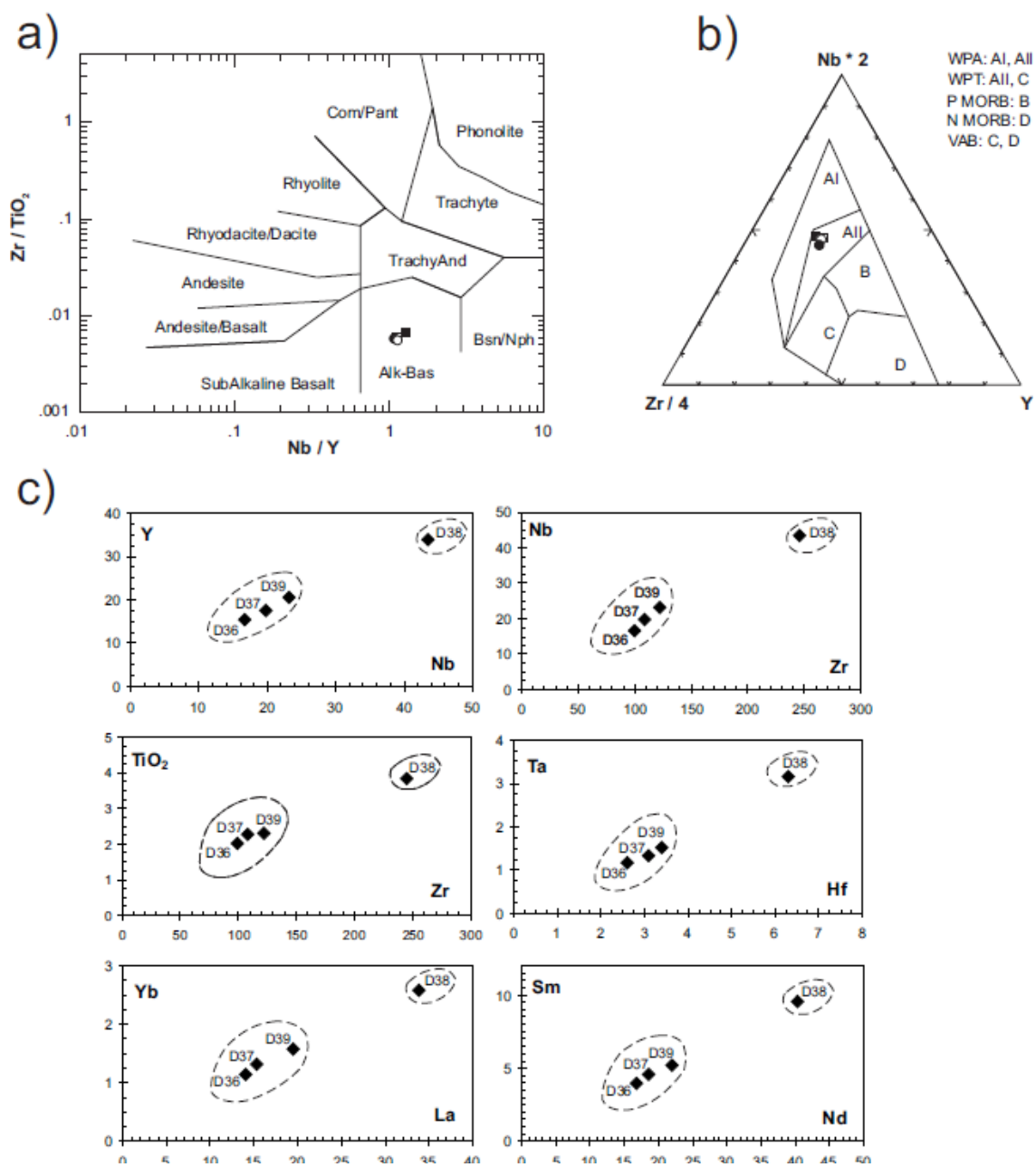
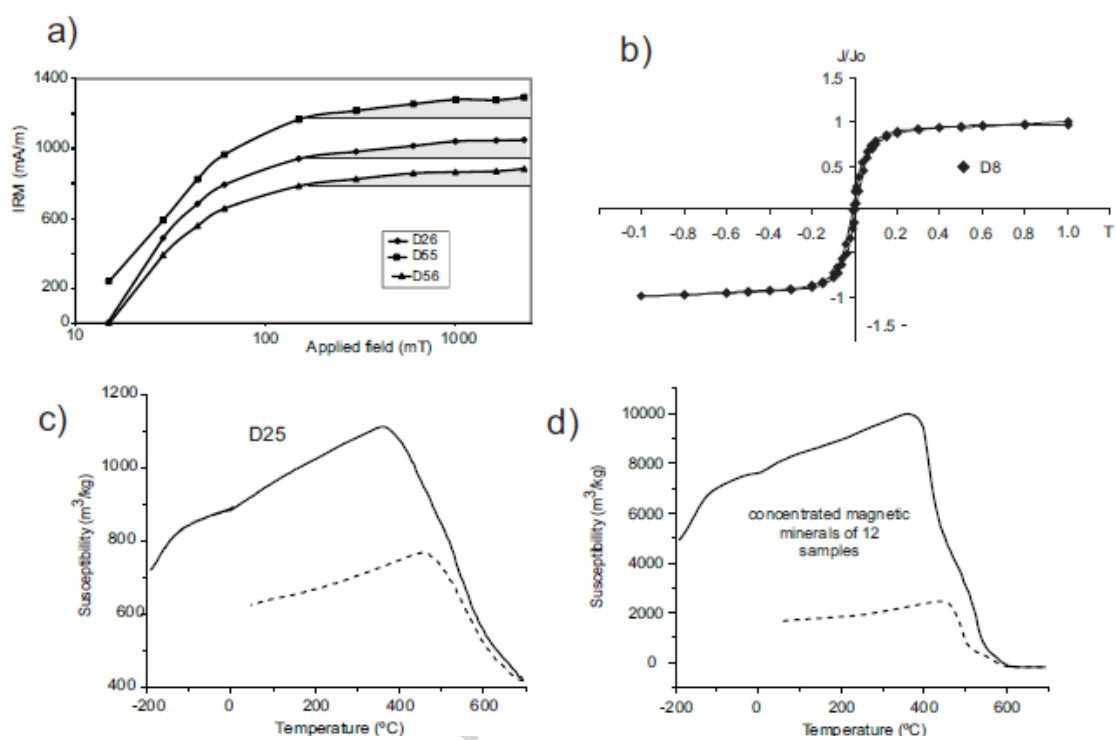
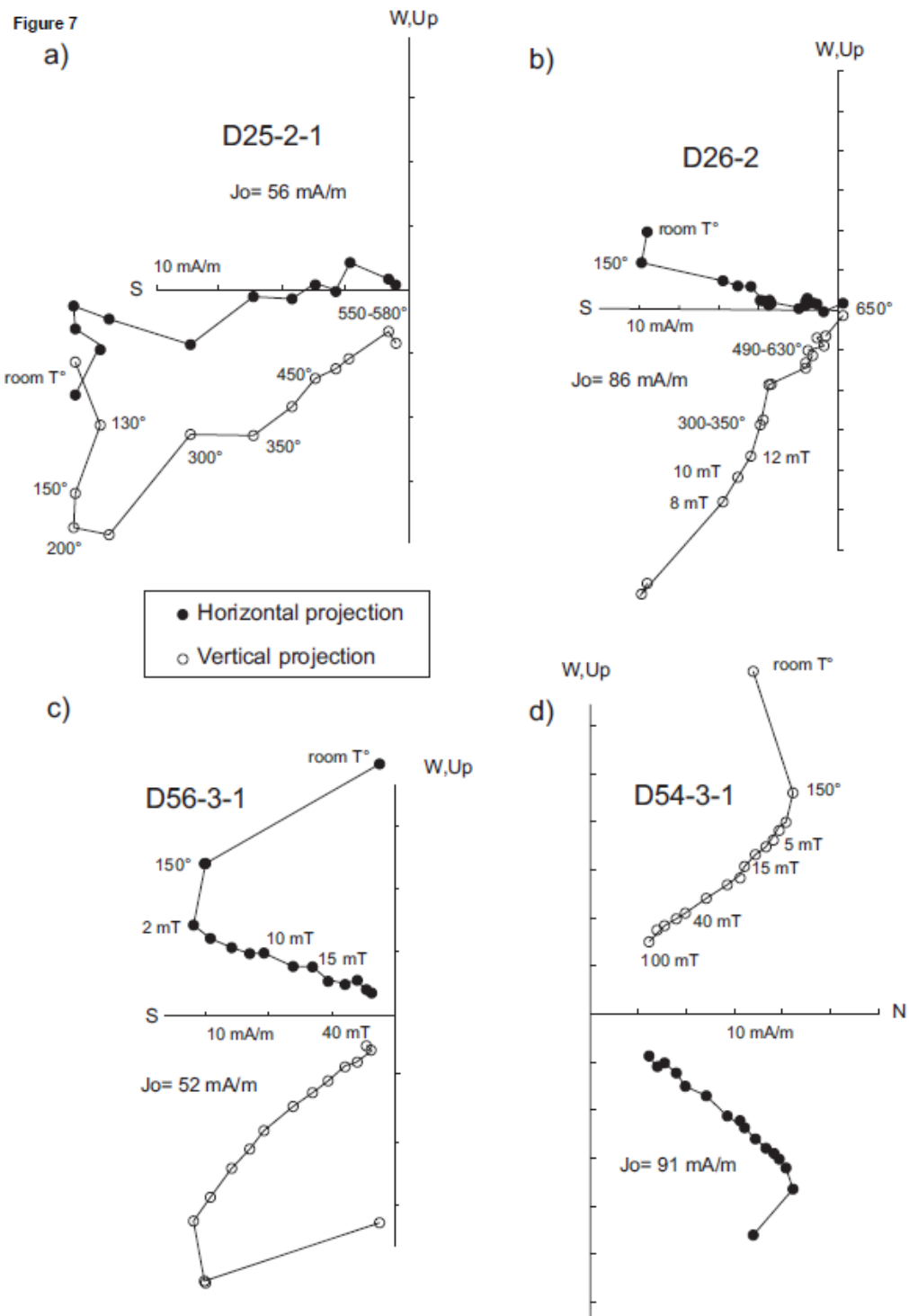


Figure 5



Figurer 6



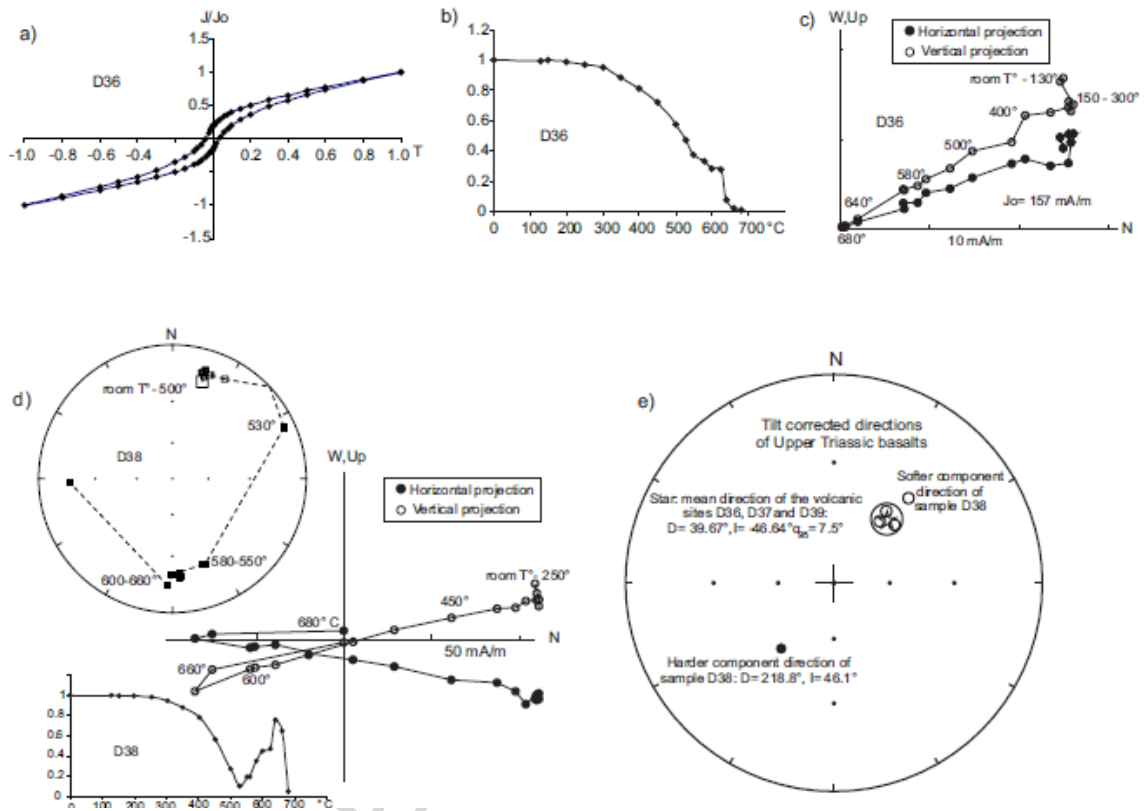


Figure 8

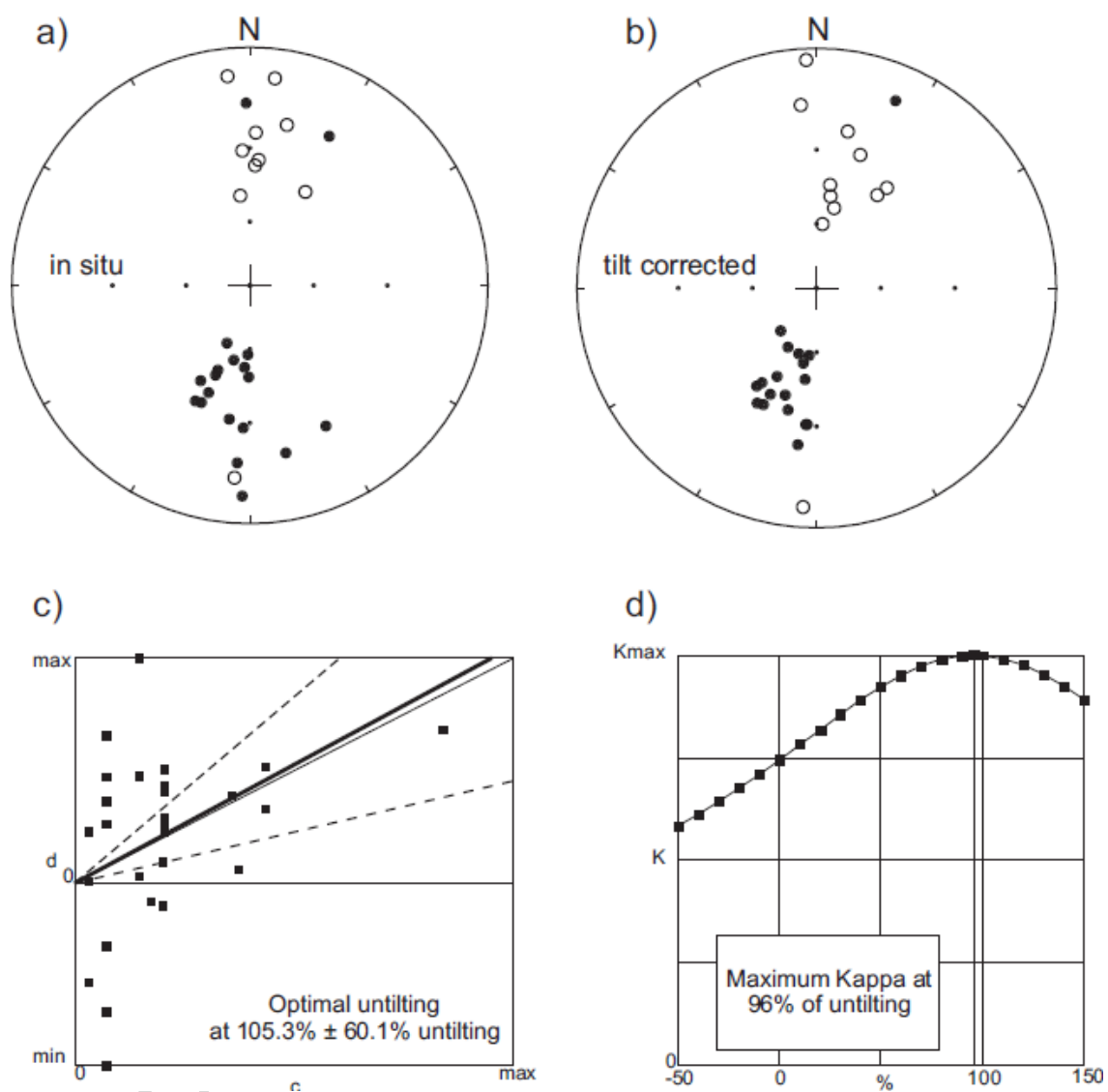


Figure 9

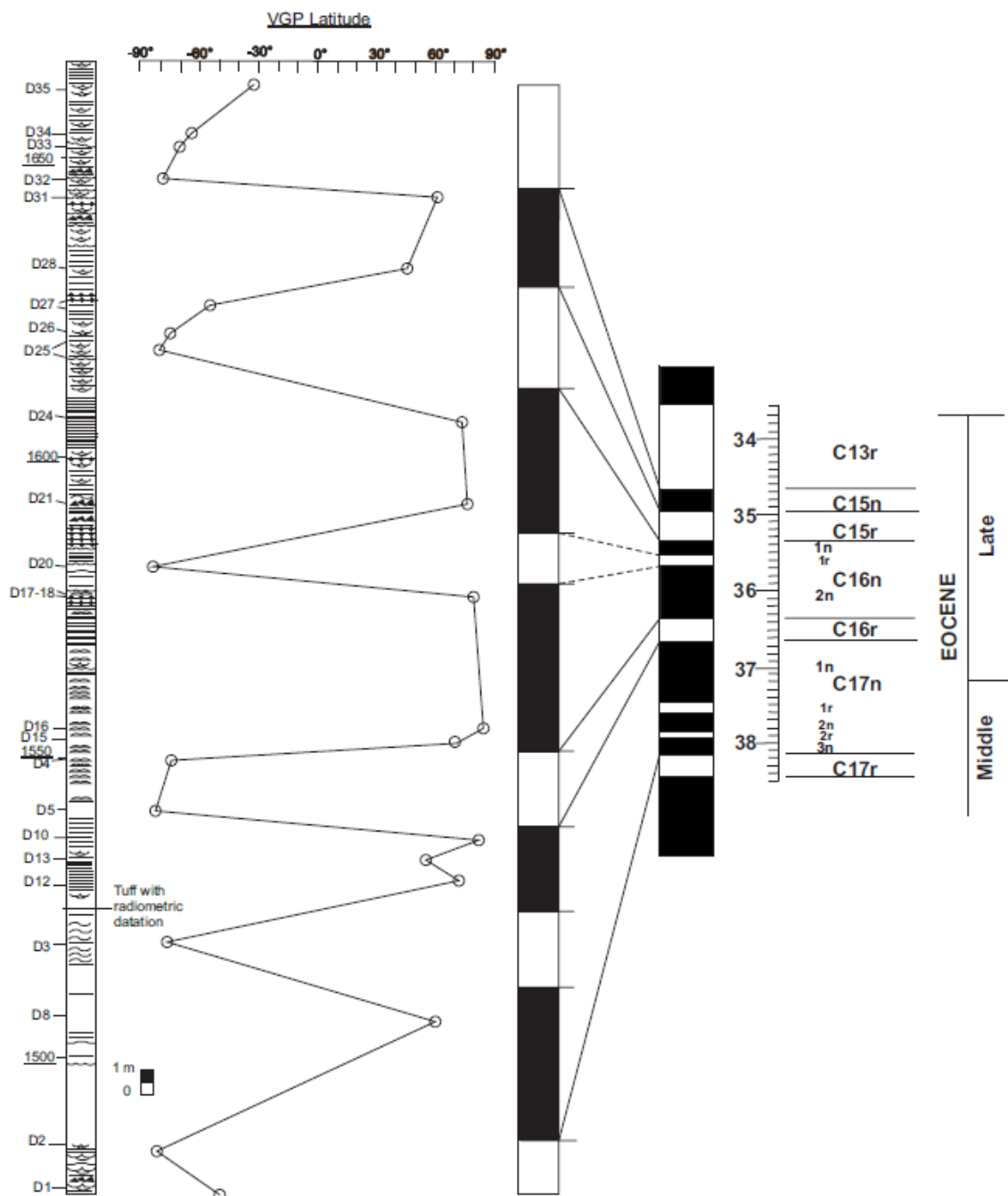


Figure 10

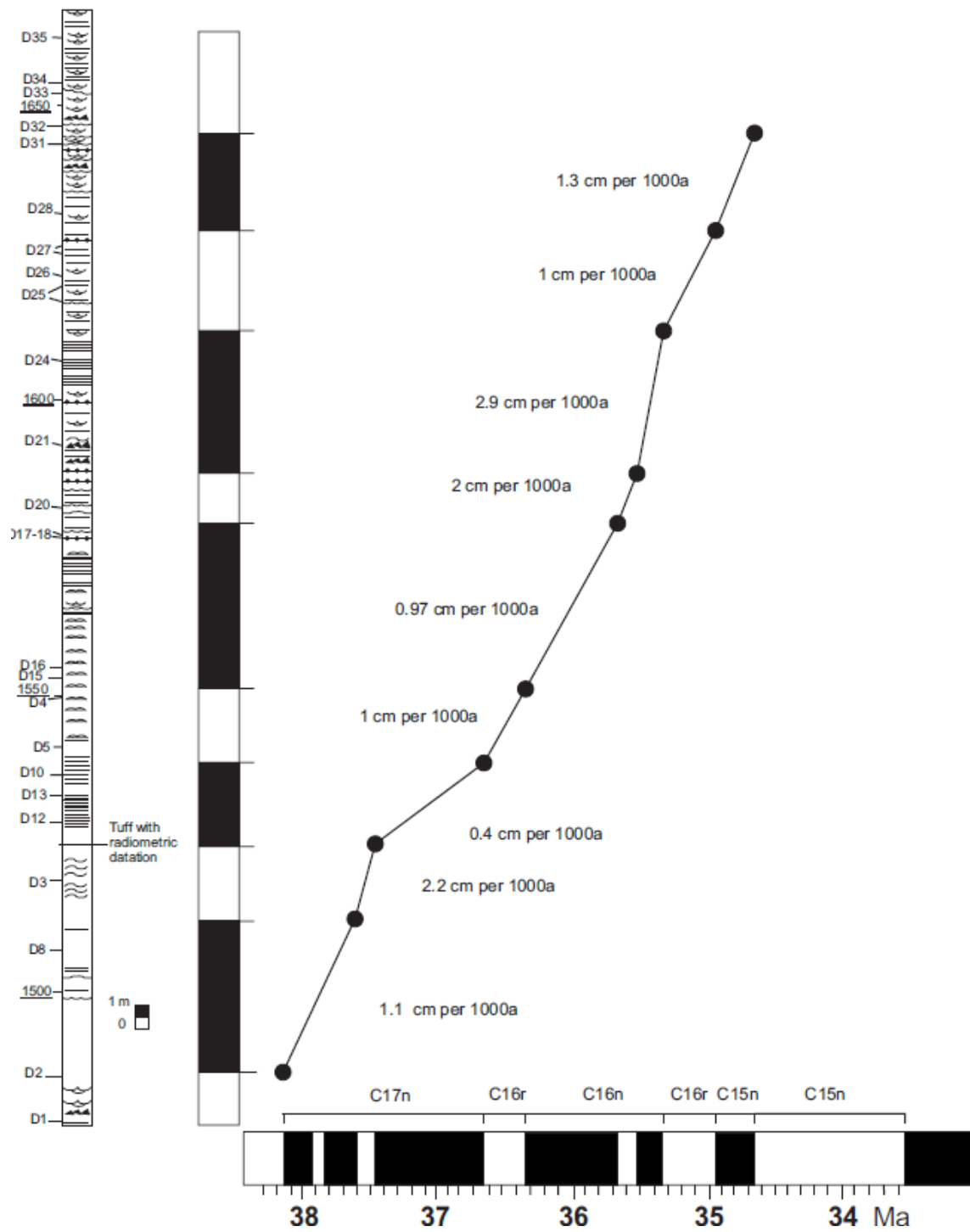


Figure 11

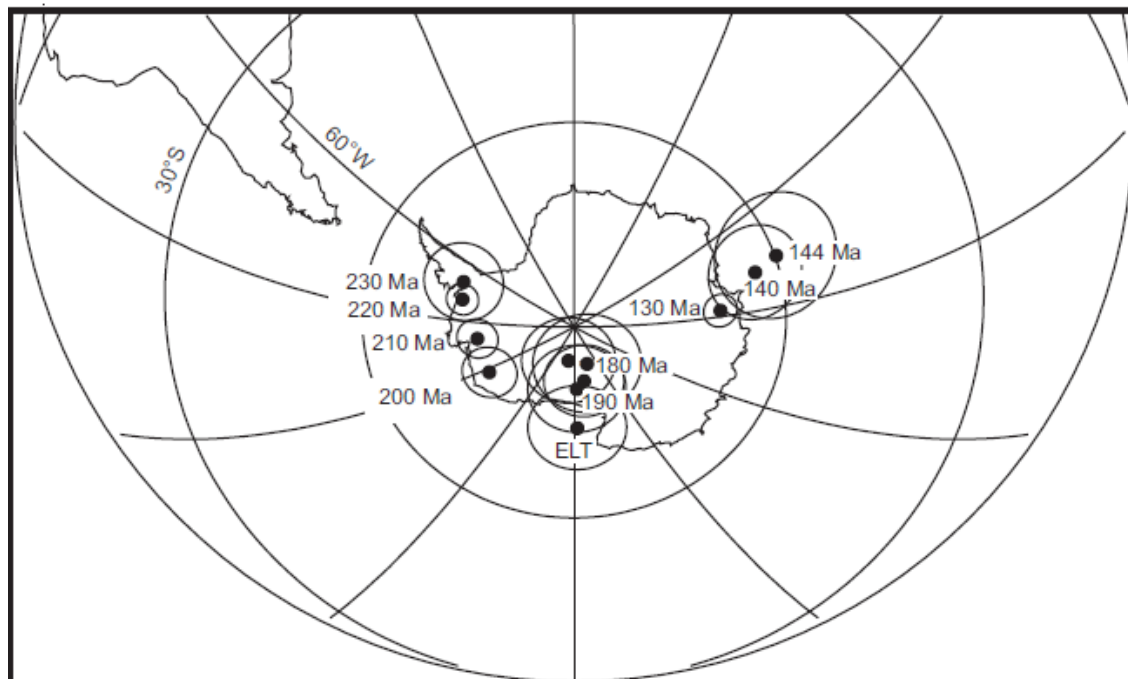


Figure 12

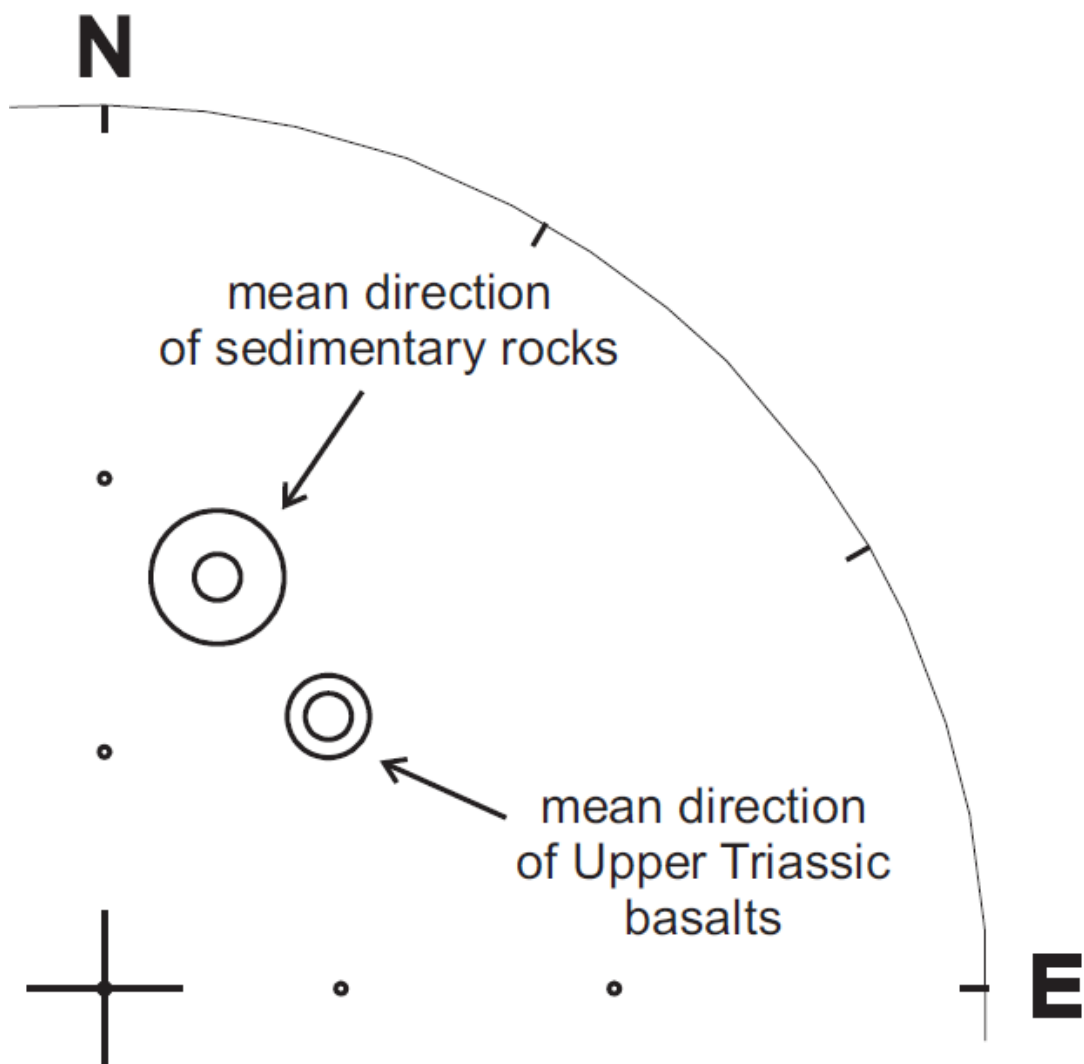


Figure 13

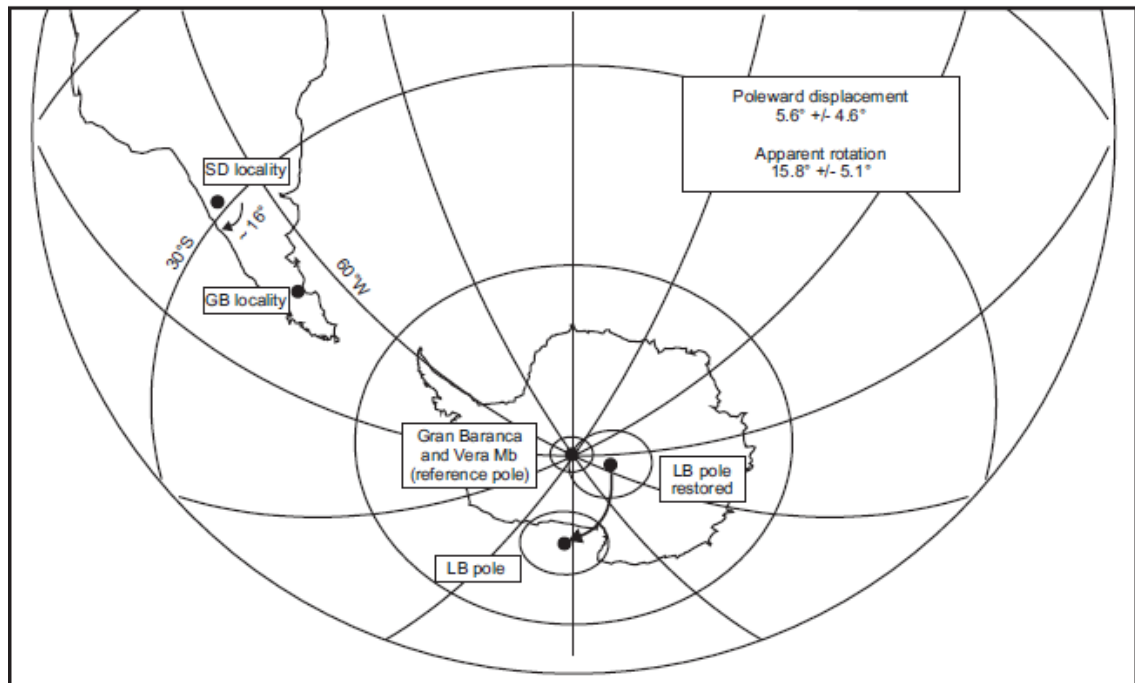


Figure 14

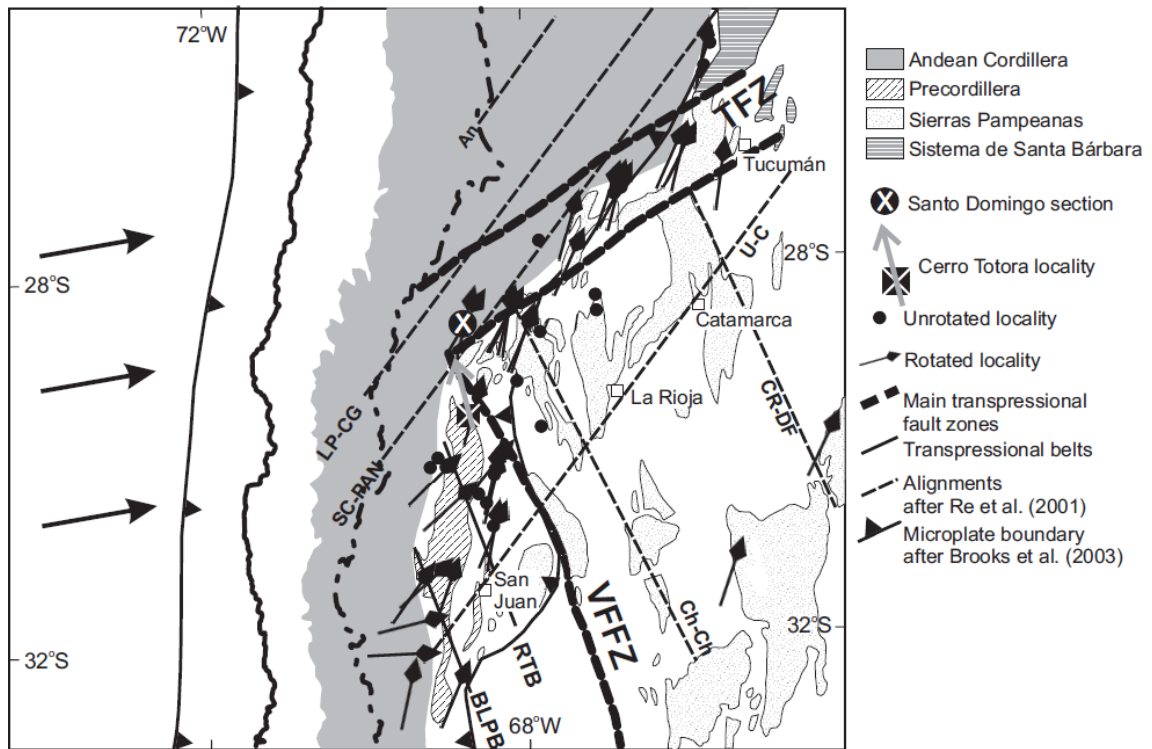


Figure 15

Highlights

- Red beds previously thought to be Triassic are actually Eocene.
- Magnetization carried by low-Ti titanomagnetite is mainly primary.
- Clockwise rotation in the boundary of Puna-Precordillera-Sierras Pampeanas.
- The unrotated pole matches the Early Jurassic APWP.
- Ambiguous interpretations arise, only resolved after precisely dating the rocks.